Electronic Supplementary Material (ESI) for Journal of Materials Chemistry A.

Supporting Information

Enhancing Proton Conductivity in a Metal-Organic Framework at T > 80 °C by Anchoring Strategy

My V. Nguyen,[a,b] Tien H. N. Lo,[a] Loc C. Luu,[c] Hue T. T. Nguyen[a] and Thach N. Tu*[a,c]

[a]Center for Innovative Materials and Architectures (INOMAR), Vietnam National University-Ho Chi Minh (VNU-HCM), Ho Chi Minh City 721337, Vietnam.

[b]University of Science, VNU-HCM, Ho Chi Minh City 721337, Vietnam.

[c]Bach Khoa University, VNU-HCM, Ho Chi Minh City 721337, Vietnam.

*To whom correspondence should be addressed: tnthach@inomar.edu.vn

Table of Contents

Section S1. Materials and Analytical Techniques

Starting Materials and General Procedures. 2,6-napthalenedicarboxylic acid (H_2NDC, 95%), zirconium chloride octahydrate ($ZrOCl_2 \cdot 8H_2O$, 98%), Histamine (His, 99%), *N*,*N*-dimethylformamide (DMF, 99% extra dry grade), sulfuric acid (H_2SO_4, 98%), hydrochloric acid (HCl, 37%) and formic acid (HCOOH, 95%) were purchased from Aldrich Chemical Co. Anhydrous methanol (MeOH, 99%) and dichloromethane (CH_2Cl_2, 99%) were obtained from Acros Organics. All other chemicals were purchased from local vendors and all chemicals were used without further purification.

Thermal gravimetric analysis (TGA) was performed on a TA Q500 thermal analysis system under air flow. Fourier transform infrared spectroscopy (FT-IR) measurements were carried out using a Bruker Vertex 70 spectrometer with the Attenuated Total Reflectance (ATR) sampling method employed. Solution ^{1}H nuclear magnetic resonance (NMR) spectra was acquired on a Bruker Advance II-500 MHz NMR spectrometer, typically, VNU-23 and $His_{8.2}\subset$VNU-23 (15 mg) were digested in 500 μL of DMSO-d_6 solution containing HF (10 μL). The mixture was then sonicated for 10 minutes before ^{1}H-NMR measurement. Water uptake measurements for pristine VNU-23, VNU-23 and $His_{8.2}\subset$VNU-23 were measured using a BELSORP-aqua3 with the experiment temperature being controlled via water circulator. Elemental analysis were performed using a LECO CHNS-932 analyzer. Impedance analysis for pelletized samples of pristine VNU-23, VNU-23 and $His_{8.2}\subset$VNU-23 (13 mm diameter, pressed at 3.76 ton.cm^{-2}) were carried out on a Gamry potentiostat (model: Interface 1000) using the two-probe method. Humidity was controlled by an Espec humidity chamber (model SH-222). The measuring frequency ranged from 1 MHz to 10 Hz. The applied voltage varied from 1 mV to 80 mV depending on open circle voltage. The thickness of the pellet was measured using a Nikon SMZ1000 microscope, with a typical pellet thickness ranging from 0.5 to 0.6 mm.

Single Crystal and Powder X-ray Diffraction Analysis. Single crystal data of pristine VNU-23 and $His_{8.2}\subset$VNU-23 were collected using Bruker four circle kappa-diffractometer equipped with a Cu INCOATED microsource, operated at 30 W power (45kV, 0.60mA) to generate Cu Kα radiation (λ = 1.54178 Å), and a Bruker VANTEC 500 area detector (microgap technology). The unit cell information was determined using Bruker APEX III

software suite. The data set was reduced and data correction was carried out by a multi-scan spherical absorption method. The structure was solved by direct methods and further refinement was performed using the full-matrix least-squares method in the SHELX-97 program package. After locating the framework backbone atoms, the SQUEEZE routine in PLATON was used to remove residual electron density from solvent molecules located within the pores of pristine VNU-23 and $His_{8.2}$⊂VNU-23. Due to the disorder of sulfonate group and the naphthalene ring, specific atoms were isotropically refined (CA22, CB22, CA34, CB34, CA16, CB16, O1, O50, S6, S7, S5, S17, S18 and related oxygen atoms bonded with sulfur atoms) and the other atoms in the structure were anisotropically refined using a modified electron density map obtained from the SQUEEZE routine. The crystallographic information file (CIF) of pristine VNU-23 can be obtained, free of charge, via the Cambridge Structural Database (CCDC number: 1585550). Similarly, due to the disorder, specific atoms was isotropically refined (histamine molecules and oxygen of sulfonate group) and the other atoms in the structure was anisotropically refined using a modified electron density map obtained from the SQUEEZE routine. The crystallographic information file (CIF) of $His_{8.2}$⊂VNU-23 can be obtained, free of charge, via the Cambridge Structural Database (CCDC number: 1810933). Powder X-ray data presented herein were collected using a Bruker D8 Advance employing Ni filtered Cu K_α (λ= 1.54178 Å). The system was equipped with an anti-scattering shield that prevents incident diffuse radiation from hitting the detector.

Section S2. ^{1}H-NMR Analysis of H_4SNDC

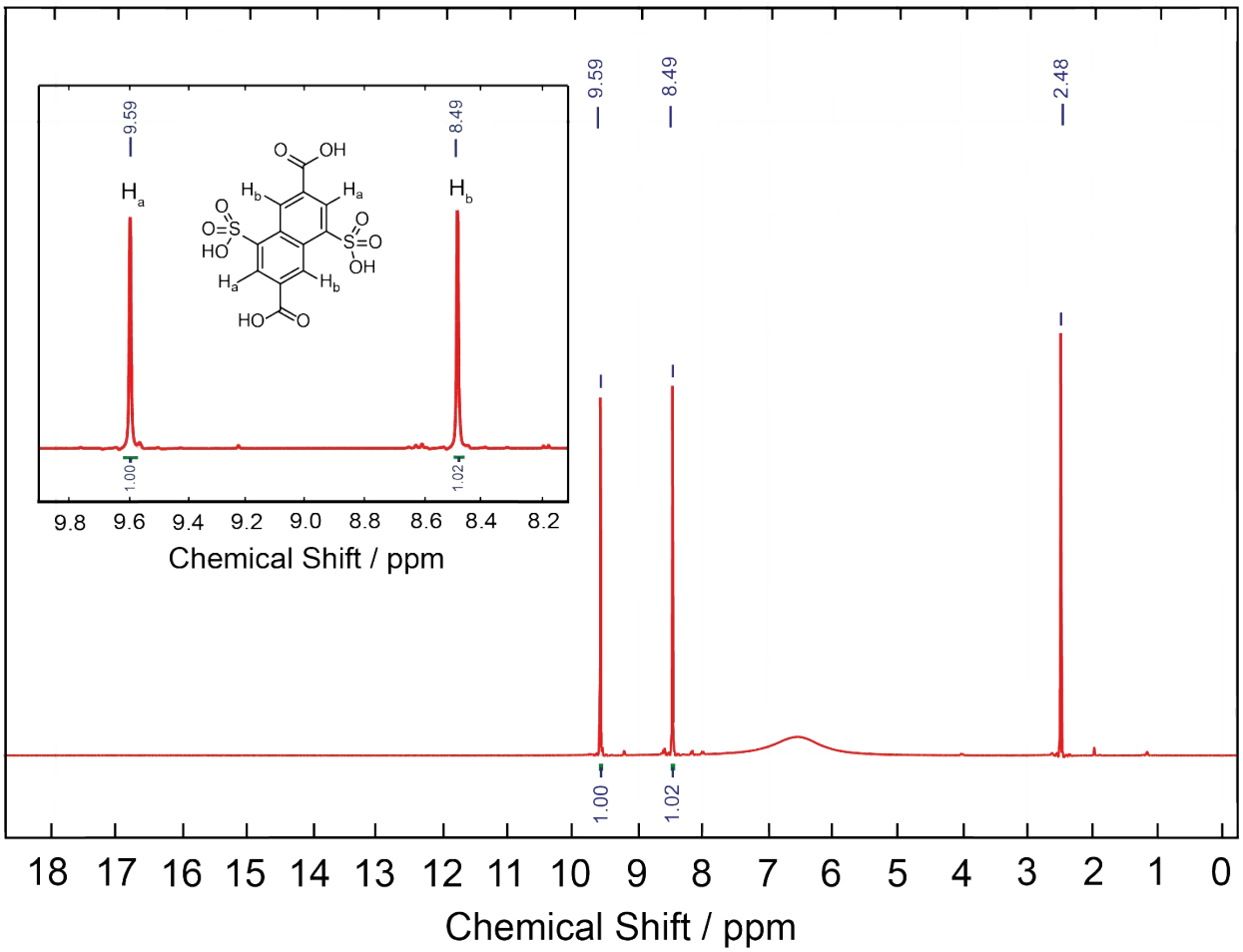

Figure S1. ^{1}H-NMR analysis of the H_4SNDC linker.

Section S3. Microscope Pictures of VNU-23

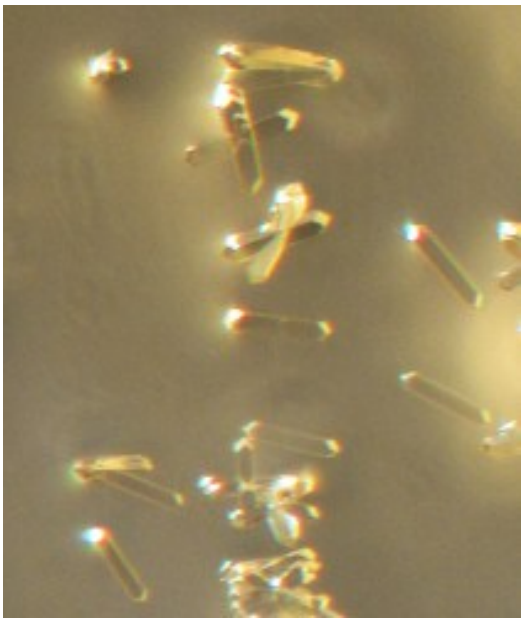

Figure S2. Optical microscopy picture of pristine VNU-23 crystals.

Section S4. Single Crystal X-ray Diffraction Analysis of VNU-23

Table S1. Crystal data and structure refinement of pristine VNU-23

Empirical formula	$C_{24}H_8O_{28}S_4Zr_3$
Formula weight	1046.2
Temperature (K)	150
Wavelength (Å)	1.54178
Crystal system	Tetragonal
Space group	*I4/m*
Unit cell dimensions (Å)	*a = 17.7174(11)*
	b = 17.7174(11)
	c = 22.4865(18)
Volume (Å^3)	7058.7(10)
Z	4
Density (g cm^{-1})	1.079
Absorption coefficient (mm^{-1})	5.183
F(000)	2240
Crystal size (mm)	0.14 × 0.05 × 0.03
θ range (°)	3.175 to 65.008.
Index ranges	$-18 \le h \le 20$, $-17 \le k \le 20$, $-26 \le l \le 18$
Reflections collected	13642
Independent reflections	3076 [R_{int}= 0.1391]
Completeness to θ = 65.008°	98.9
Data / restraints / parameters	13642 / 9 / 167
S (GOF)	0.939
R_1, wR_2 [$I > 2\sigma(I)$]	0.0714, 0.1898
R_1, wR_2 (all data)	0.1150, 0.2149
Largest diff. peak and hole (e·Å^{-3})	1.065 and -0.988

Section S5. Powder X-ray Diffraction Patterns

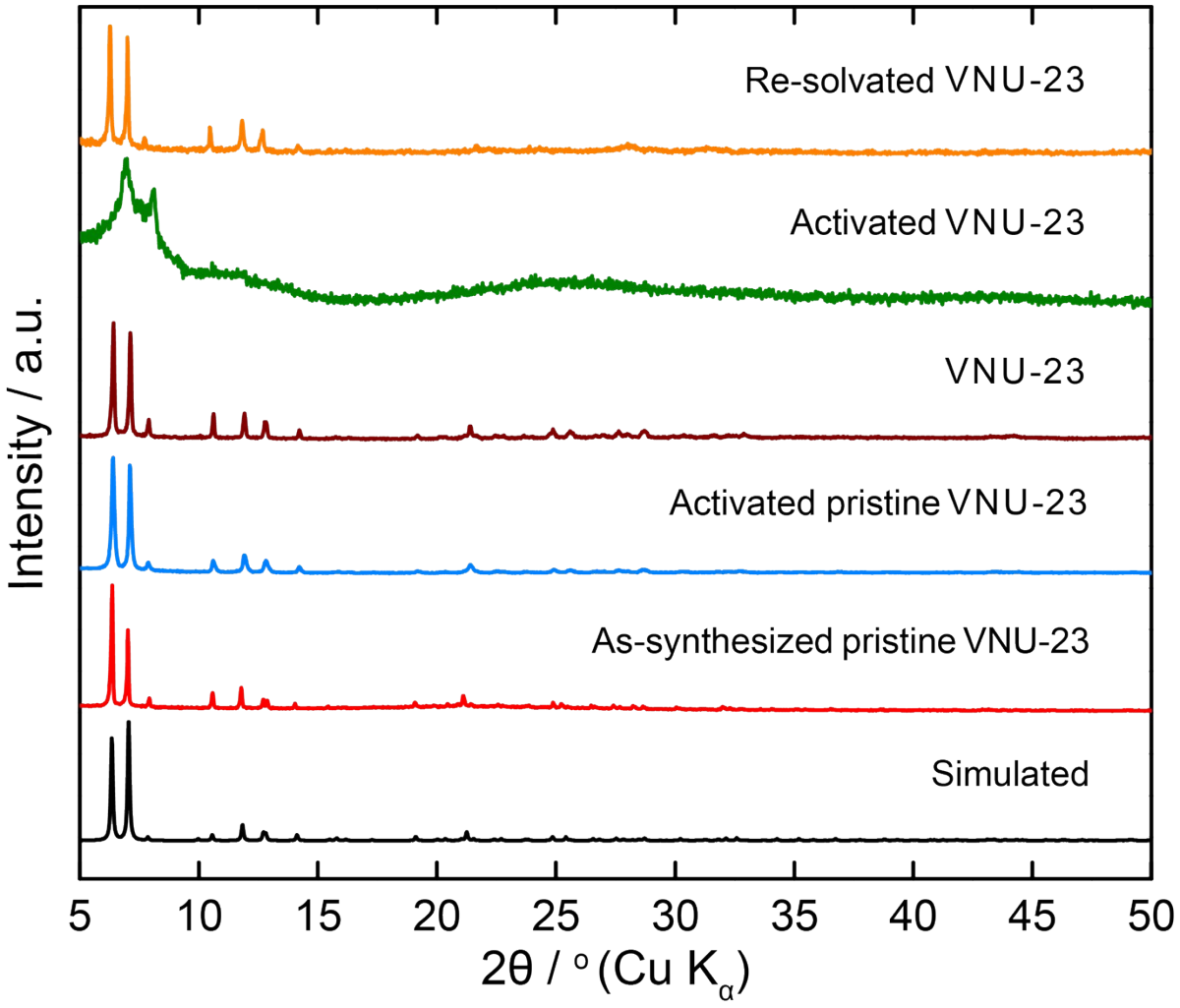

Figure S3. Powder X-ray diffraction patterns of VNU-23 after multistep-steps preparation.

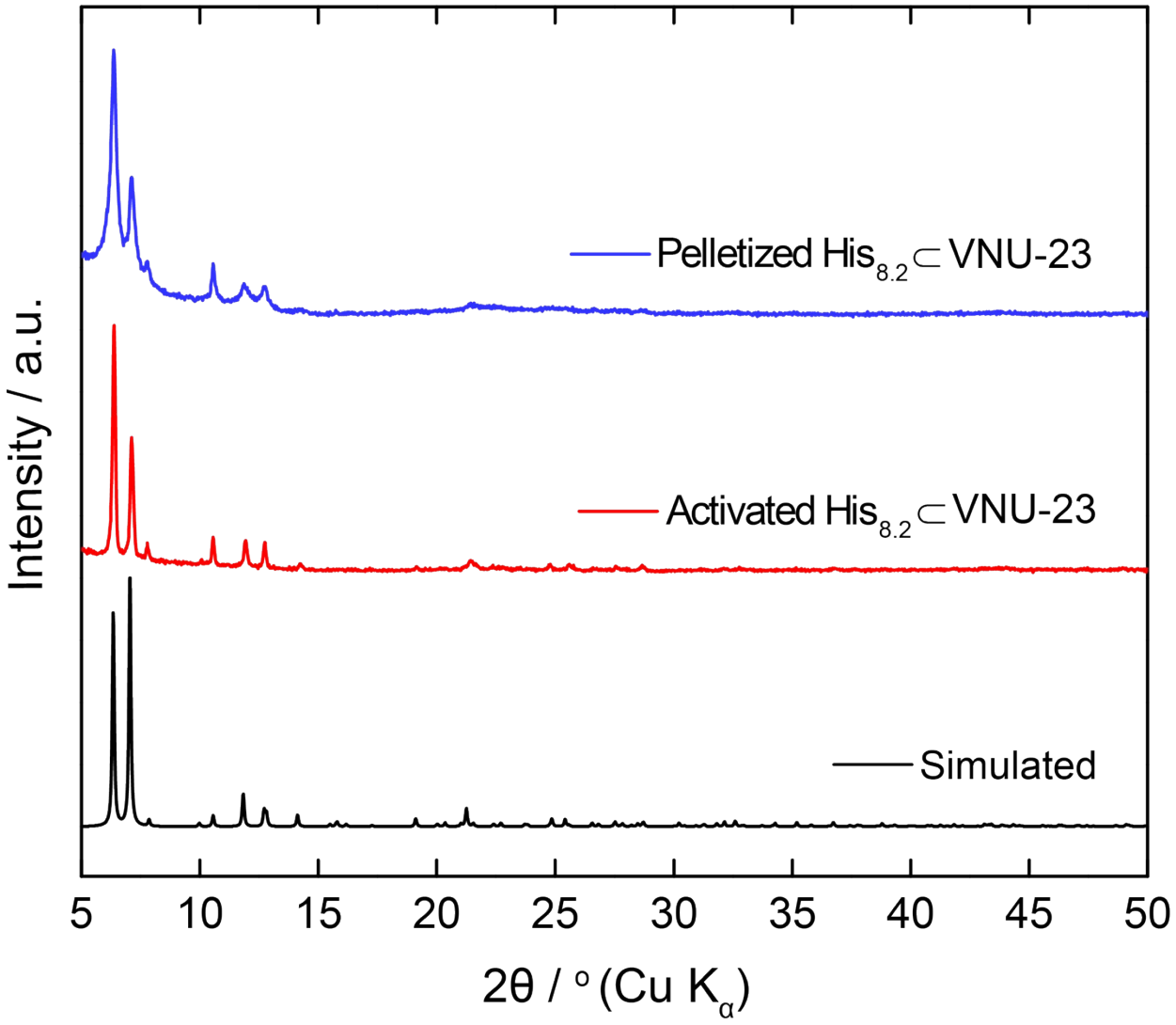

Figure S4. Powder X-ray diffraction patterns of activated $His_{8.2}$⊂VNU-23 and pelletized $His_{8.2}$⊂VNU-23 pressing at 3.76 tons cm^{-2}.

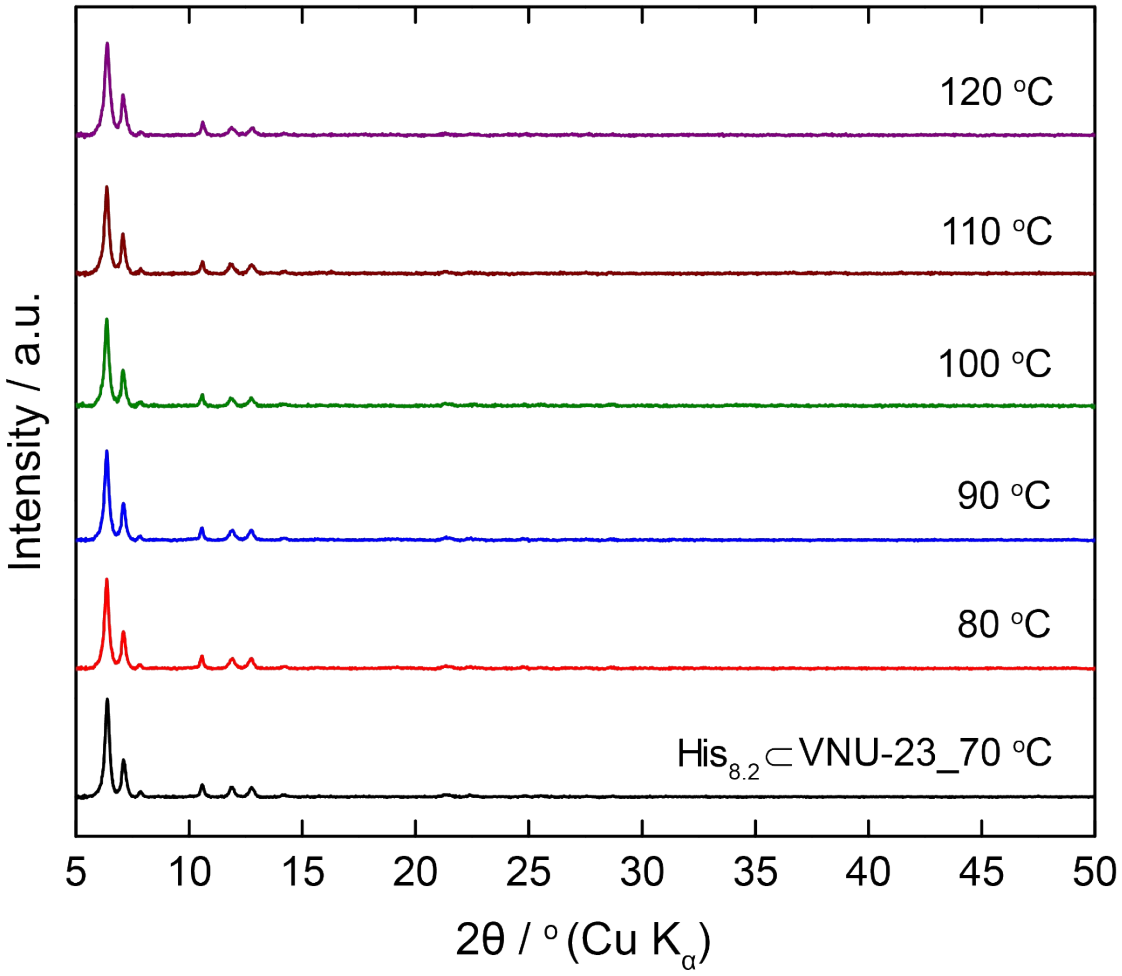

Figure S5. Temperature-dependent PXRD analysis of activated $His_{8.2}$⊂VNU-23 from 70 to 120 °C.

Section S6. Fourier Transform Infrared Analysis (FT-IR)

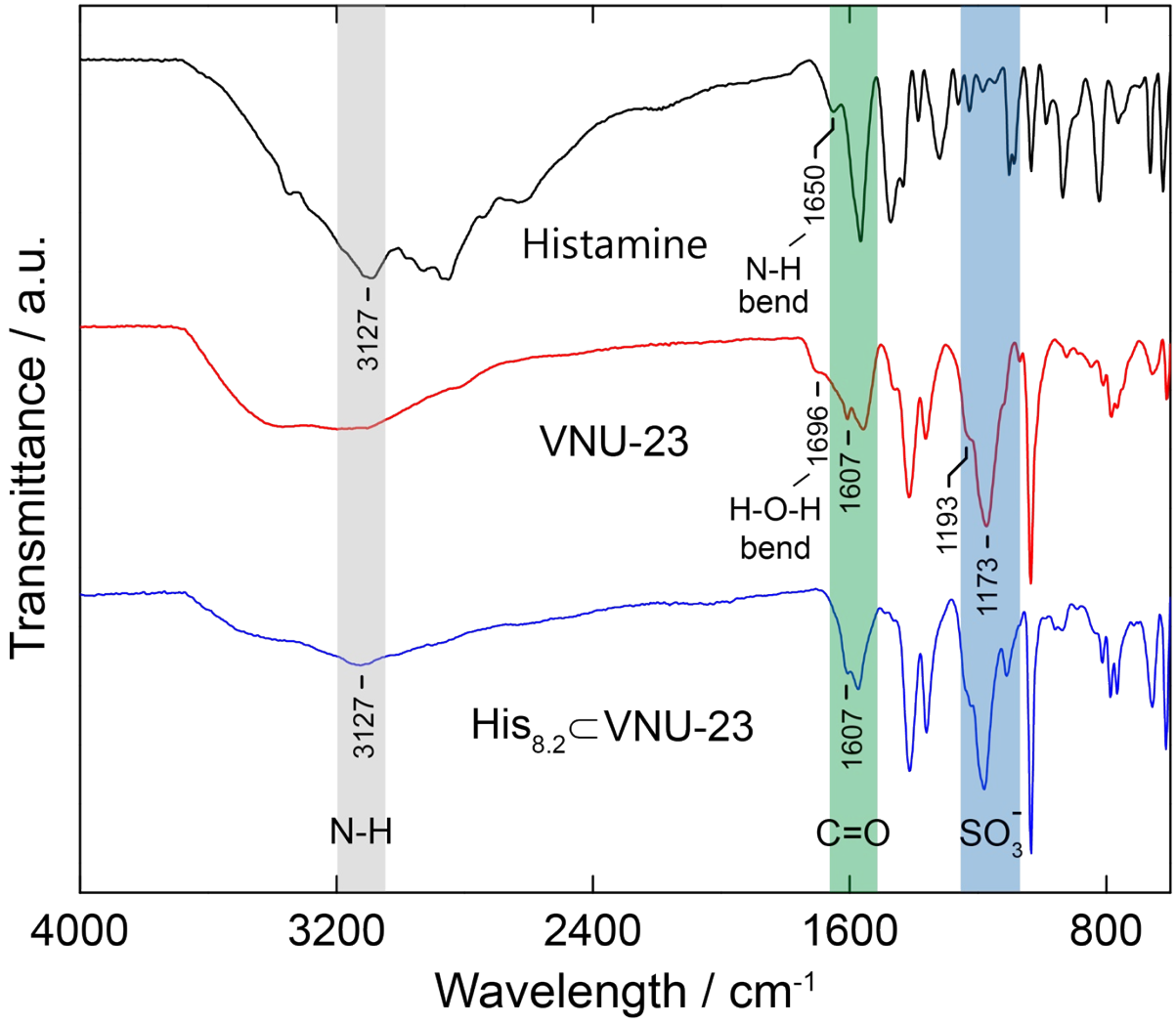

Figure S6. Fourier transform infrared analysis (FT-IR) of VNU-23, $His_{8.2}$⊂VNU-23 and bulk histamine.

Section S7. Thermal Gravimetric Analysis (TGA)

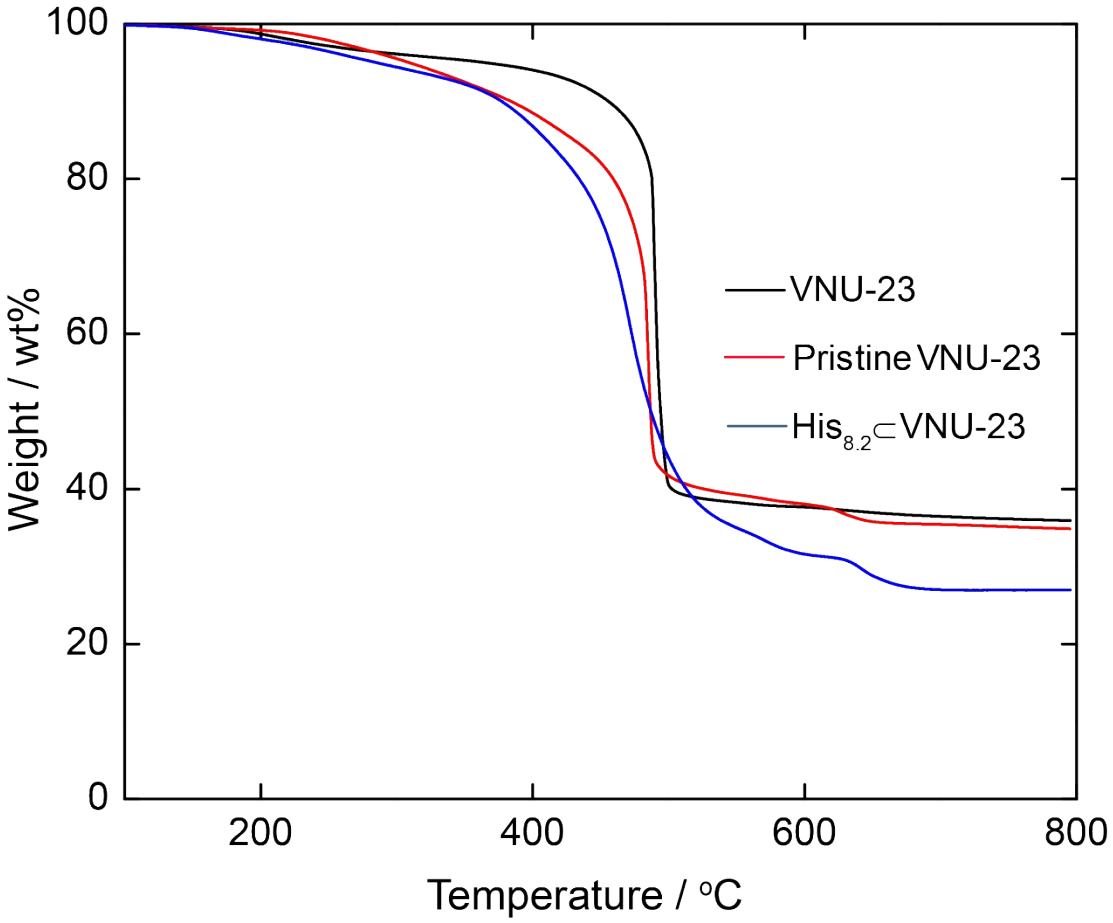

Figure S7. TGA analysis of pristine VNU-23, VNU-23 and $His_{8.2}$⊂VNU-23.

Section S8. N_2 Adsorption Isotherm of VNU-23 and $His_{8.2}$⊂VNU-23

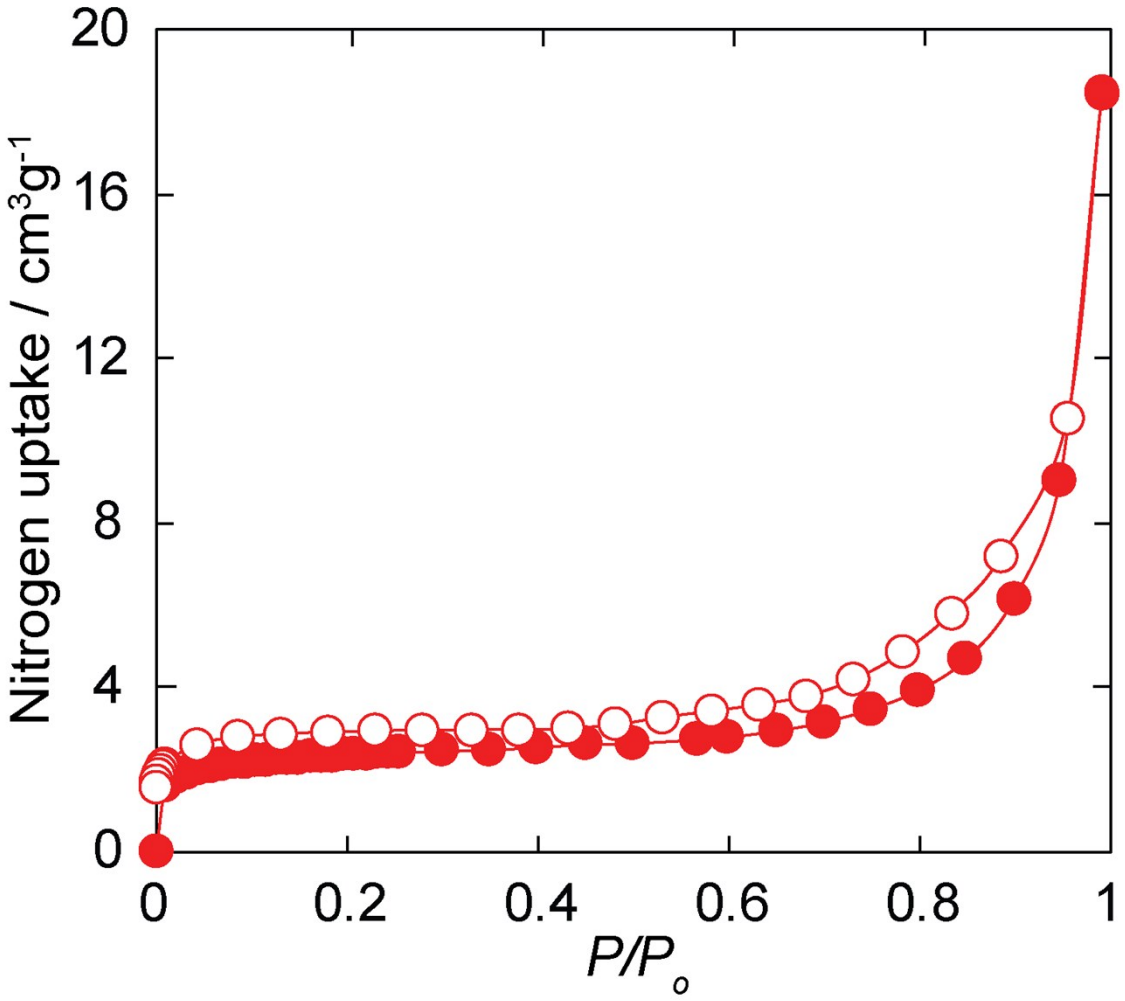

Figure S8. N_2 uptake of VNU-23 at 77 K. The closed and open circles represent the adsorption and desorption branches of the isotherm, respectively.

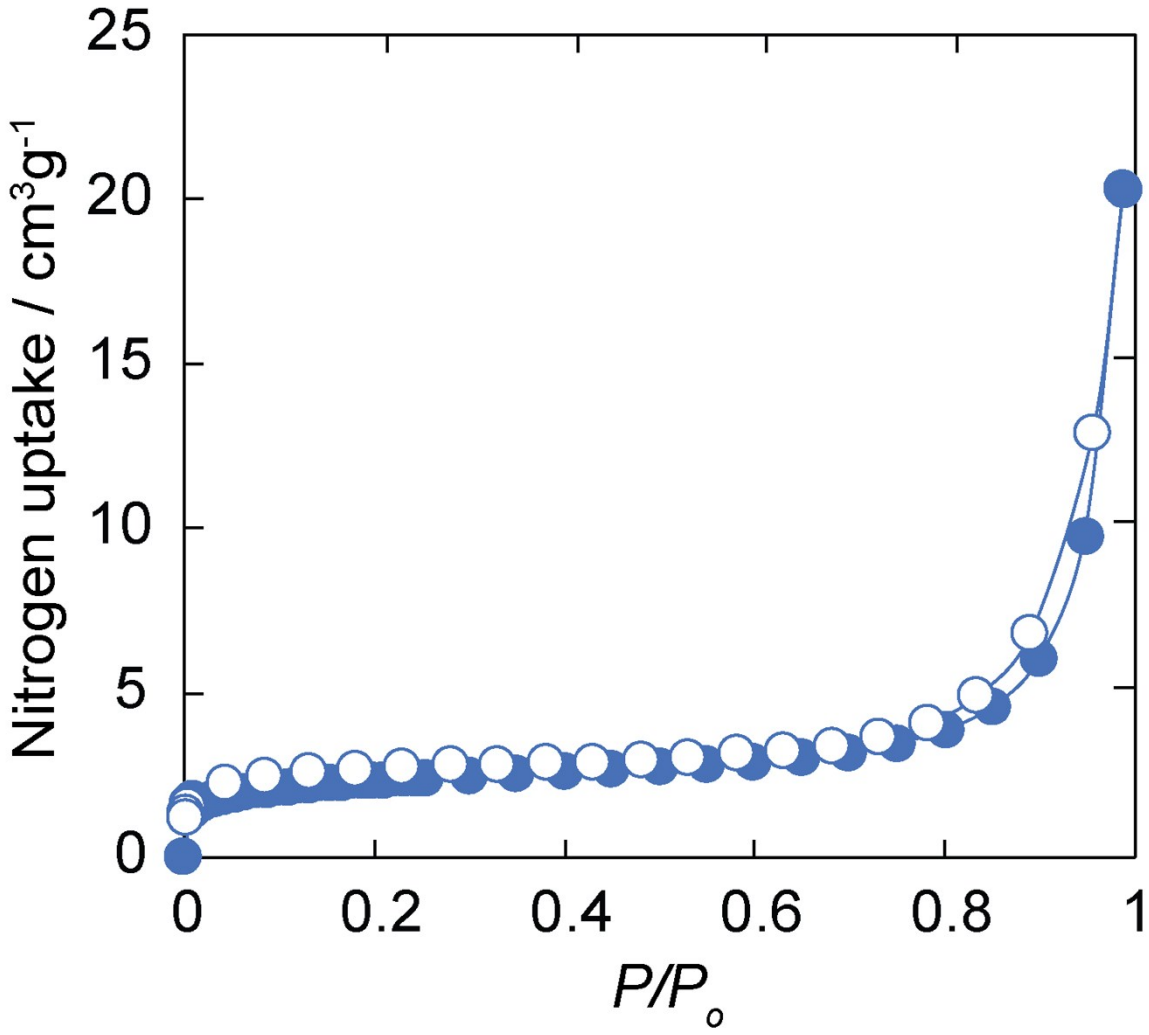

Figure S9. N_2 uptake of $His_{8.2}$⊂VNU-23 at 77 K. The closed and open circles represent the adsorption and desorption branches of the isotherm, respectively.

Section S9. Stability of VNU-23 in Water

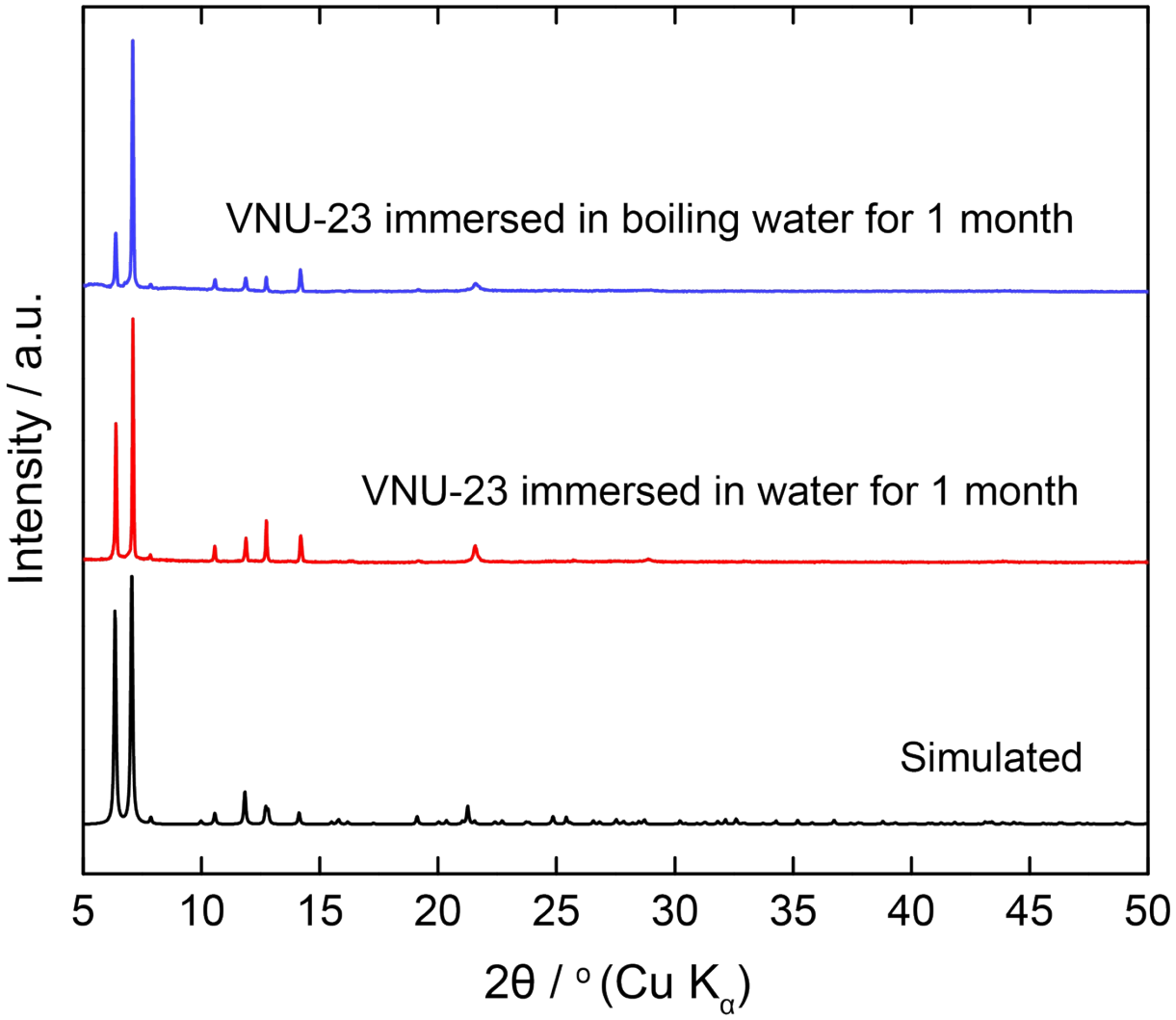

Figure S10. Powder X-ray diffraction patterns of VNU-23 in water for one month.

Section S10. ^{1}H-NMR Analysis of Digested Samples

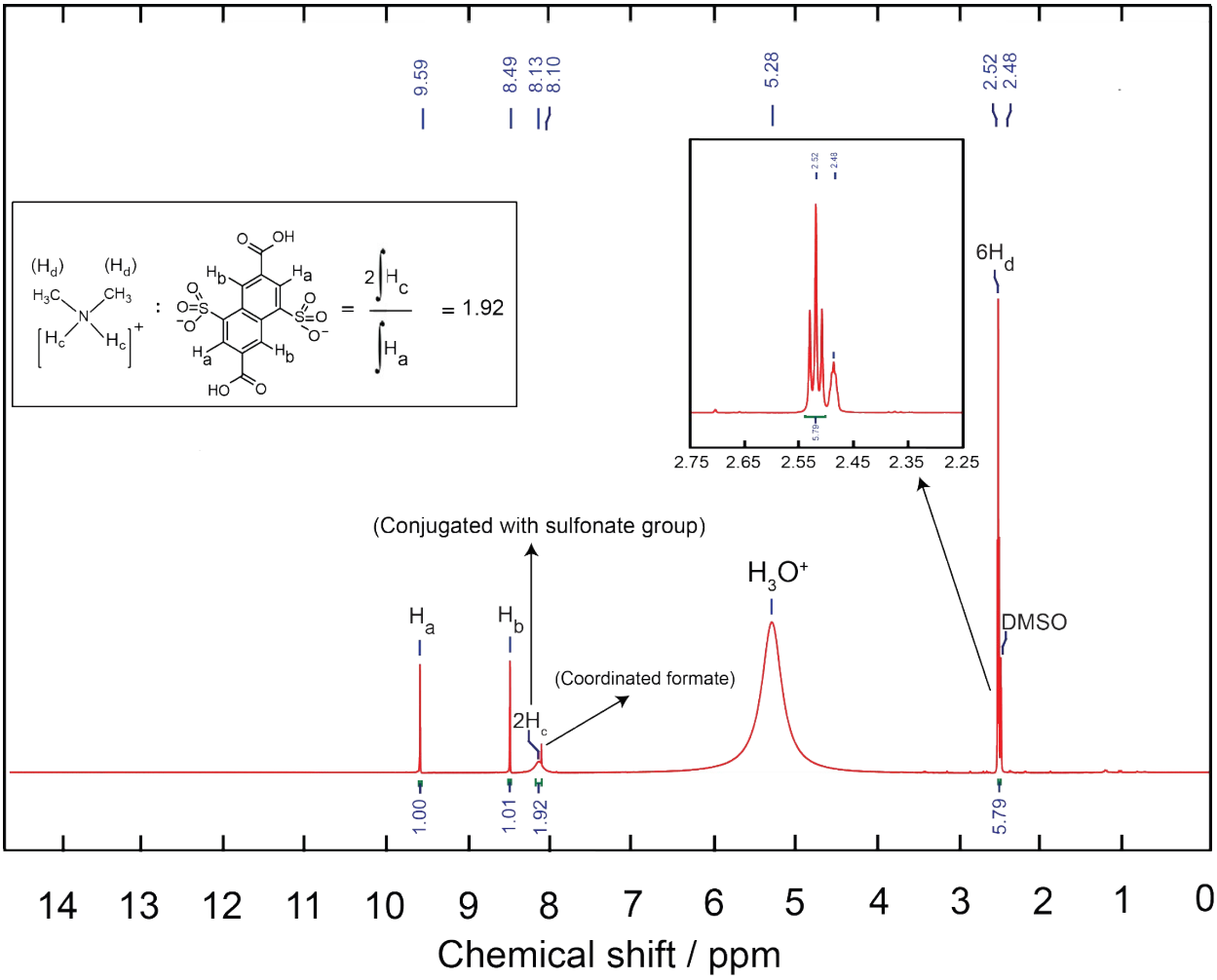

Figure S11. ^{1}H-NMR analysis of digested pristine VNU-23. The peak, at 8.13 ppm, was attributed to the protons of amine group (dimethylamonium), which is in the conjugation with sulfonate group. This peak is not observed without the presence of sulfonate group. Additionally, the protons of amine group (δ = 8.13 ppm) interacted with CH_3 group (H_d), led to the triplet peak at 2.52 ppm.

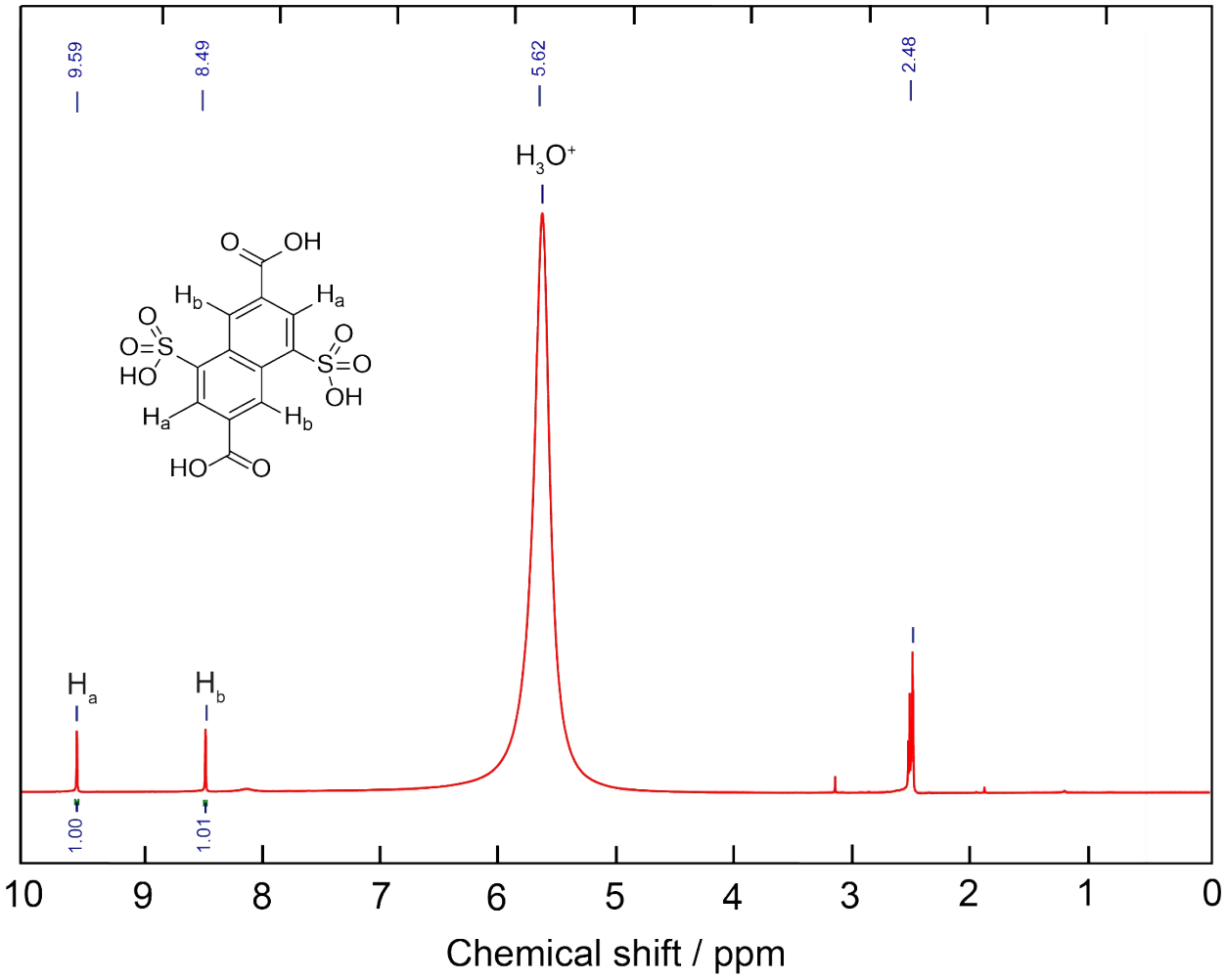

Figure S12. ^{1}H-NMR analysis of digested VNU-23.

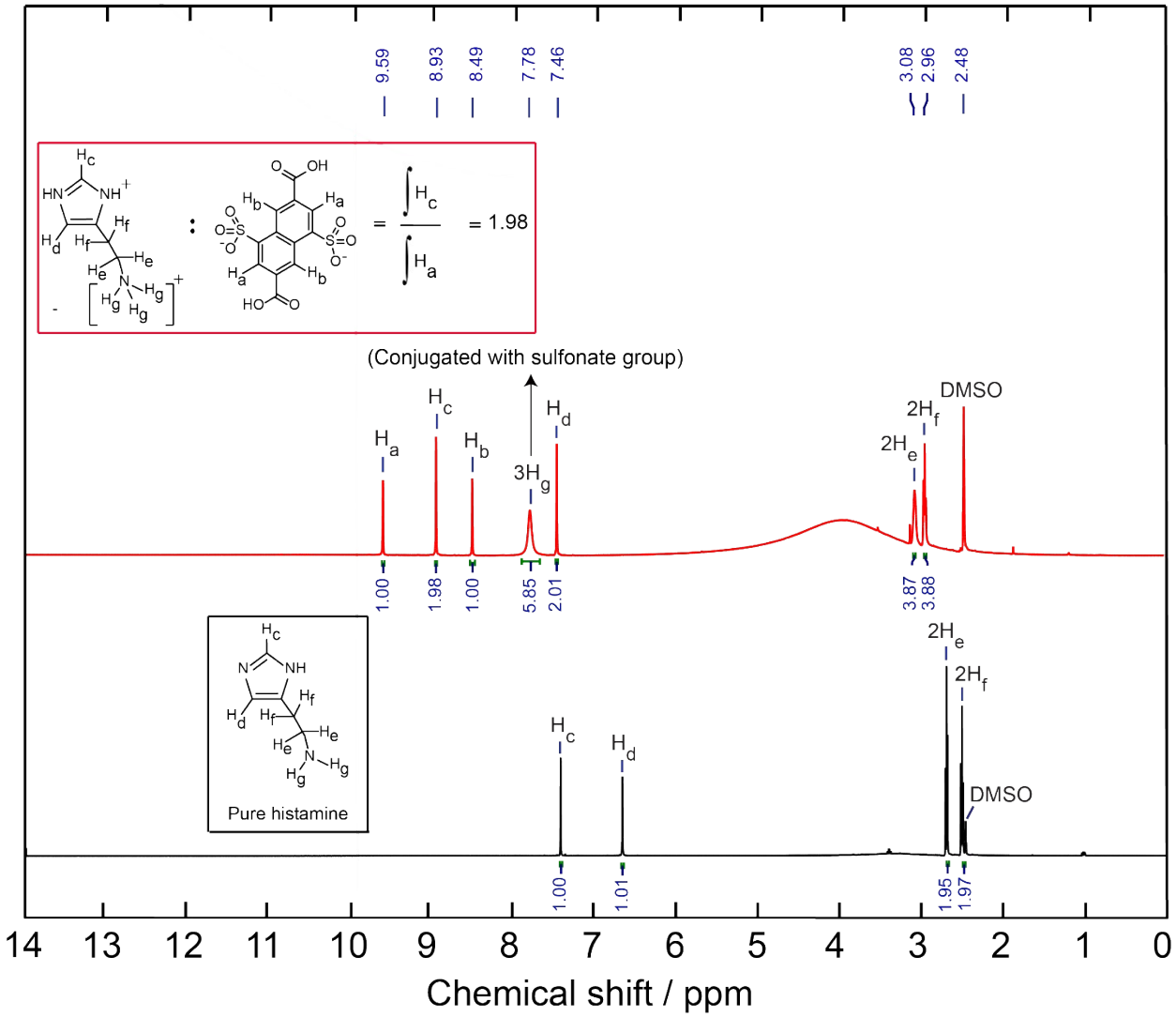

Figure S13. ^{1}H-NMR analysis of digested $His_{8.2}$⊂VNU-23 in contrast with ^{1}H-NMR from pure histamine. The ^{1}H-NMR peaks of the protons in protonated histamine was observed to center at higher chemical shift in comparison with pure histamine. This phenomenon was assigned to effect, caused by the protonation of histamine.

Section S11. Water Adsorption Studies

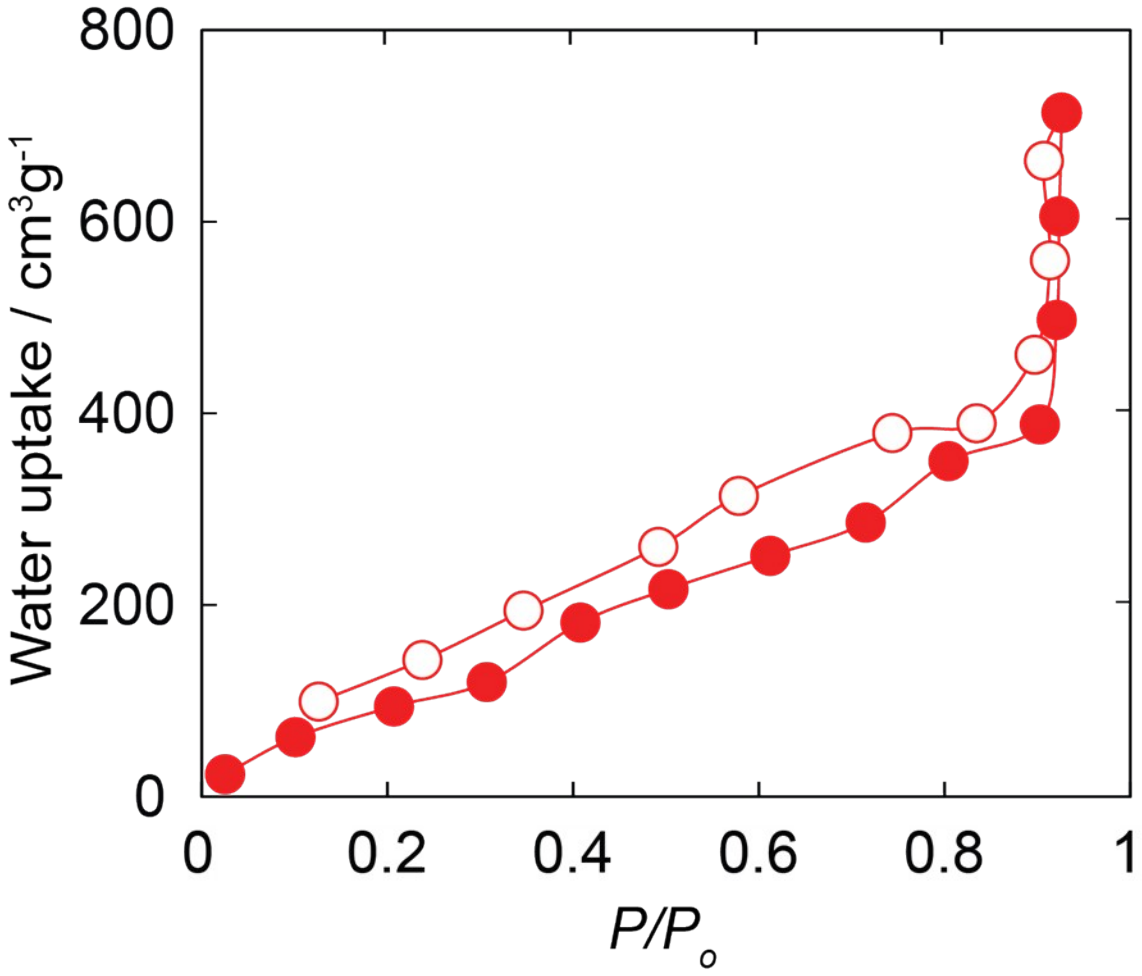

Figure S14. Water uptake of pristine VNU-23 at 25 °C as a function of P/P_0.

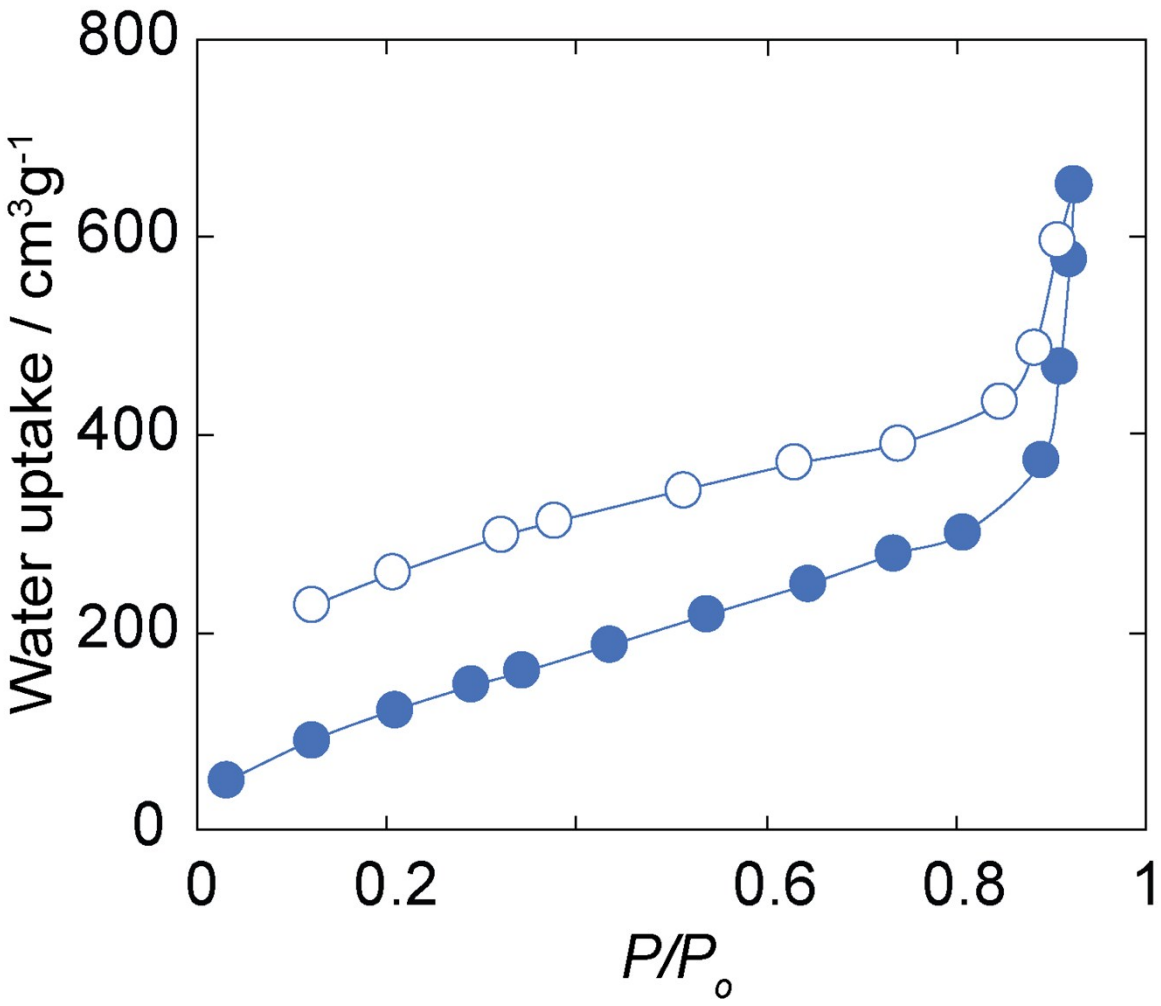

Figure S15. Water uptake of VNU-23 at 25 °C as a function of P/P_0.

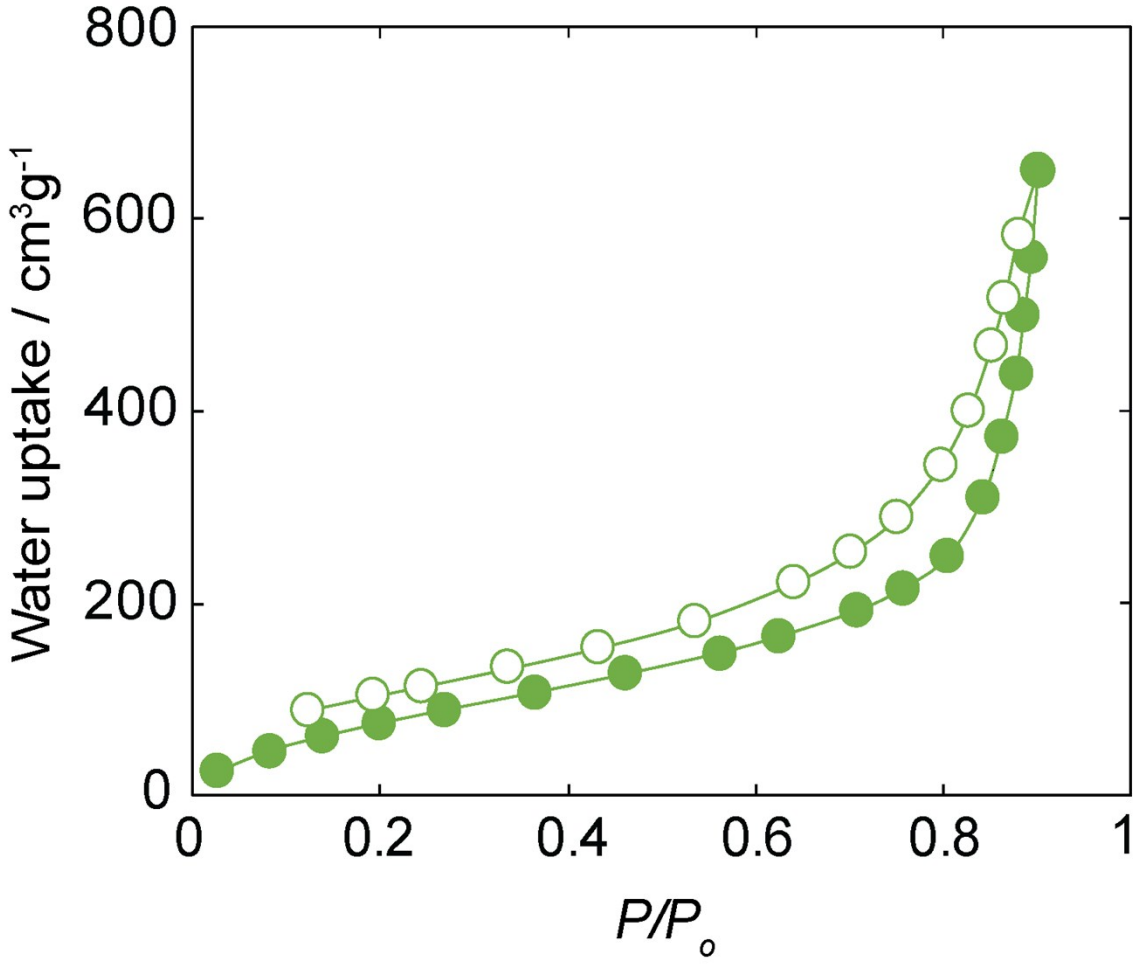

Figure S16. Water uptake of $His_{8.2}$⊂VNU-23 at 25 °C as a function of P/P_0.

Section S12. Stability of $His_{8.2}$⊂VNU-23 during Water Adsorption

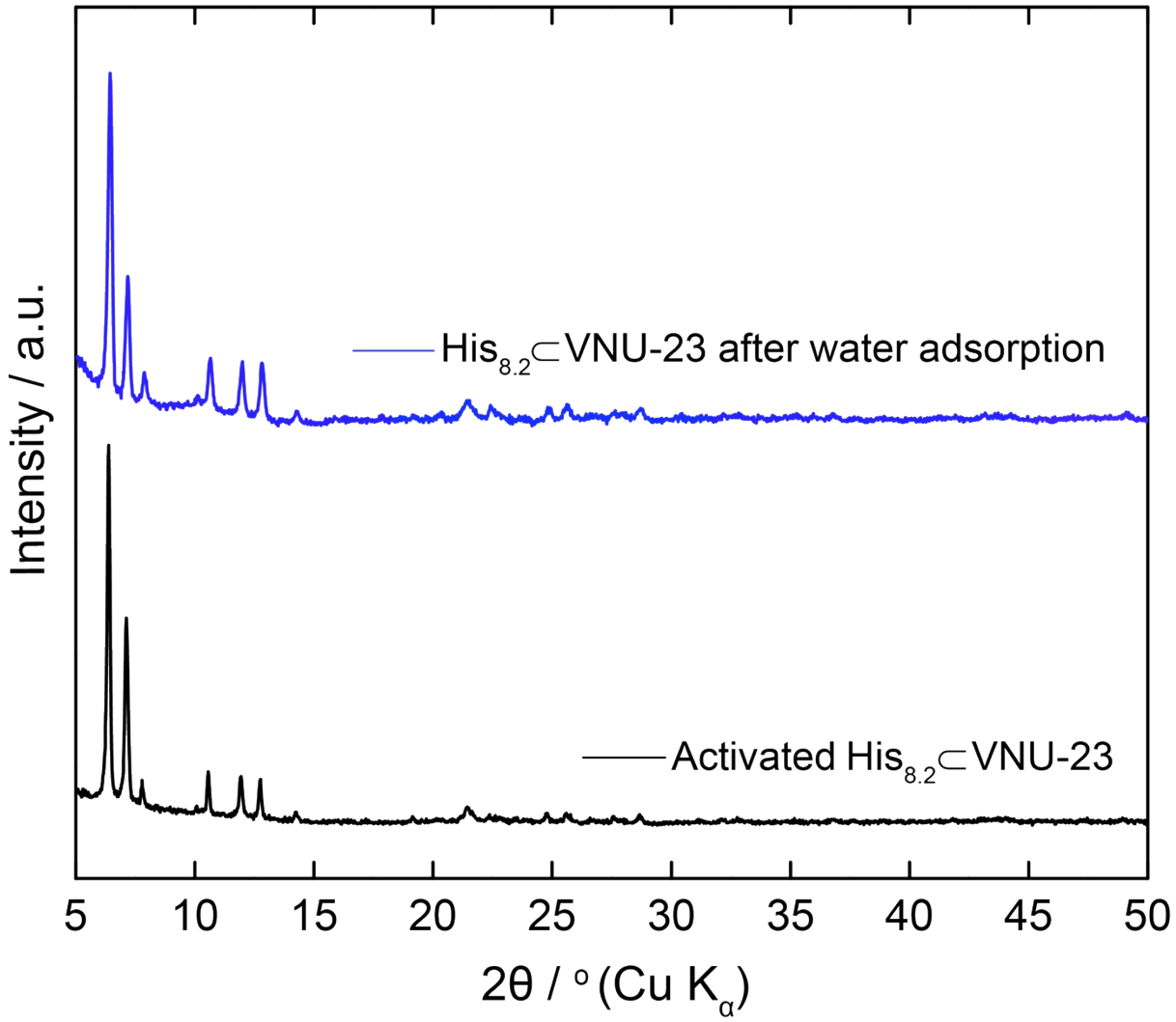

Figure S17. Activated PXRD pattern of $His_{8.2}$⊂VNU-23 (black) as compared to $His_{8.2}$⊂VNU-23 after water adsorption at 25 °C (blue).

Section S13. Single Crystal X-ray Diffraction Analysis of $His_{8.2}$⊂VNU-23

Table S2. Crystal data and structure refinement of $His_{8.2}$⊂VNU-23

Empirical formula	$C_{27}H_8N_{1.80}O_{28}S_4Zr_3$
Formula weight	1212.89
Temperature (K)	150
Wavelength (Å)	1.54178
Crystal system	Tetragonal
Space group	*I4/m*
Unit cell dimensions (Å)	*a = 17.526(3)* *b = 17.526(3)* *c = 22.893(3)*
Volume (Å^3)	7032(2)
Z	4
Density (g cm^{-1})	1.141
Absorption coefficient (mm^{-1})	5.235
F(000)	2362
Crystal size (mm)	0.10 × 0.03 × 0.03
θ range (°)	3.176 to 61.160.
Index ranges	-19 ≤ *h* ≤ 19, -16 ≤ *k* ≤ 16, -25 ≤ *l* ≤ 24
Reflections collected	13797
Independent reflections	2750 [R_{int}= 0.1537]
Completeness to *θ* = 61.160°	98.6
Data / restraints / parameters	13797/ 51 / 241
S (GOF)	1.002
R_1, wR_2 [$I > 2\sigma(I)$]	0.0896, 0.2752
R_1, wR_2 (all data)	0.1287, 0.2333
Largest diff. peak and hole (e·Å^{-3})	1.123 and -1.456

Section S14. Proton Conduction Study

It is noted that the impedance of the electric wire without pelleted sample was collected in order to correct for the inductive effect. The correction was carried out by subtracting the experimental impedance of pelletized sample from the experimental impedance of the electric wire in order to obtain the pure impedance of pelletized sample.

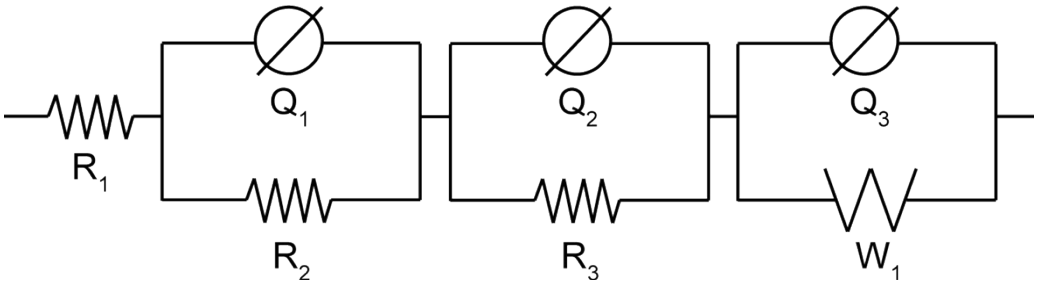

Figure S18. An equivalent circuit used for fitting. Schematic representations: W_1, Warburg diffusion element; $Q_1/Q_2/Q_3$, imperfect capacitor; R_1, Contact resistor; R_2, bulk resistor; R_3, grain boundary resistor.

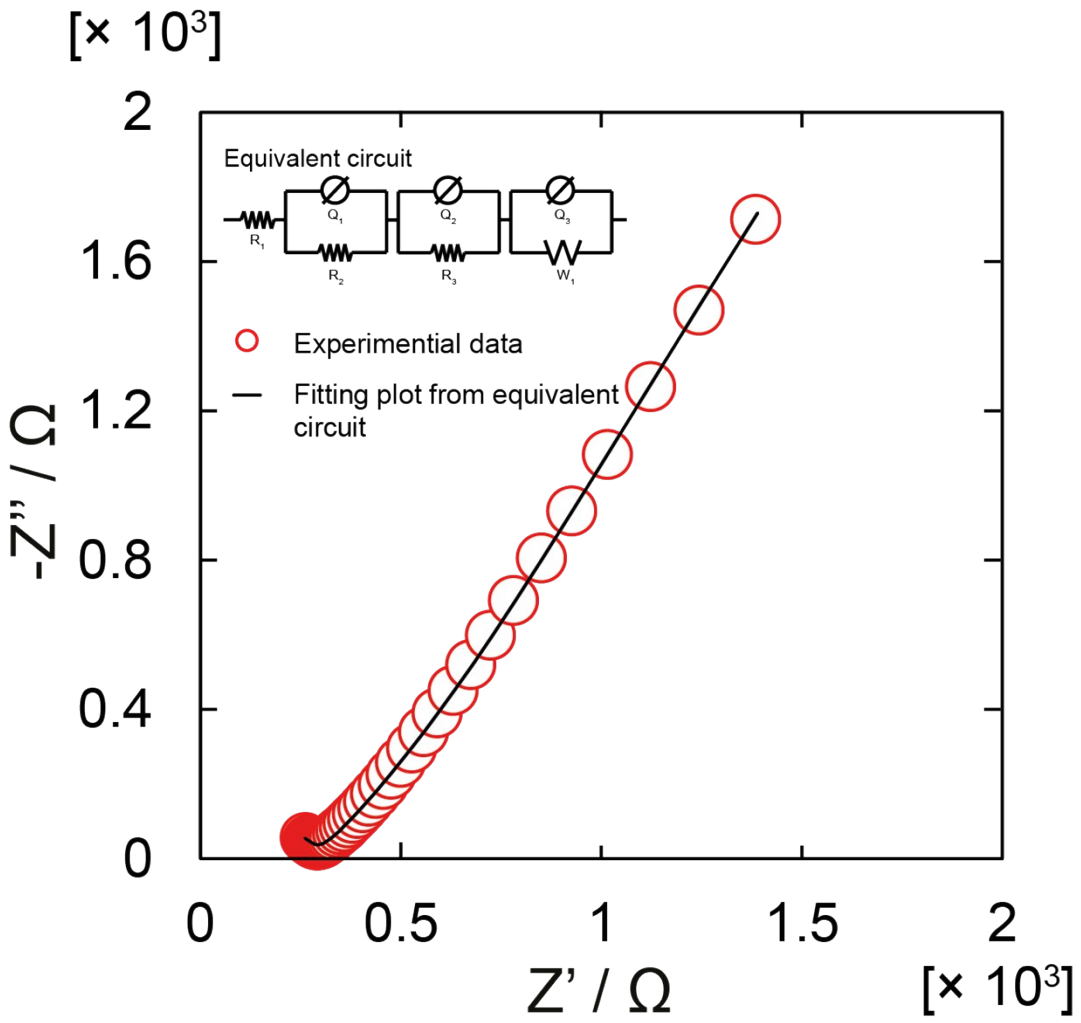

Figure S19. Nyquist plot derived from equivalent circuit (black line) and experimental Nyquist plot (red circles) of pelletized pristine VNU-23 under 90% RH and 70 °C. Frequency ranged from 1 MHz to 10 Hz.

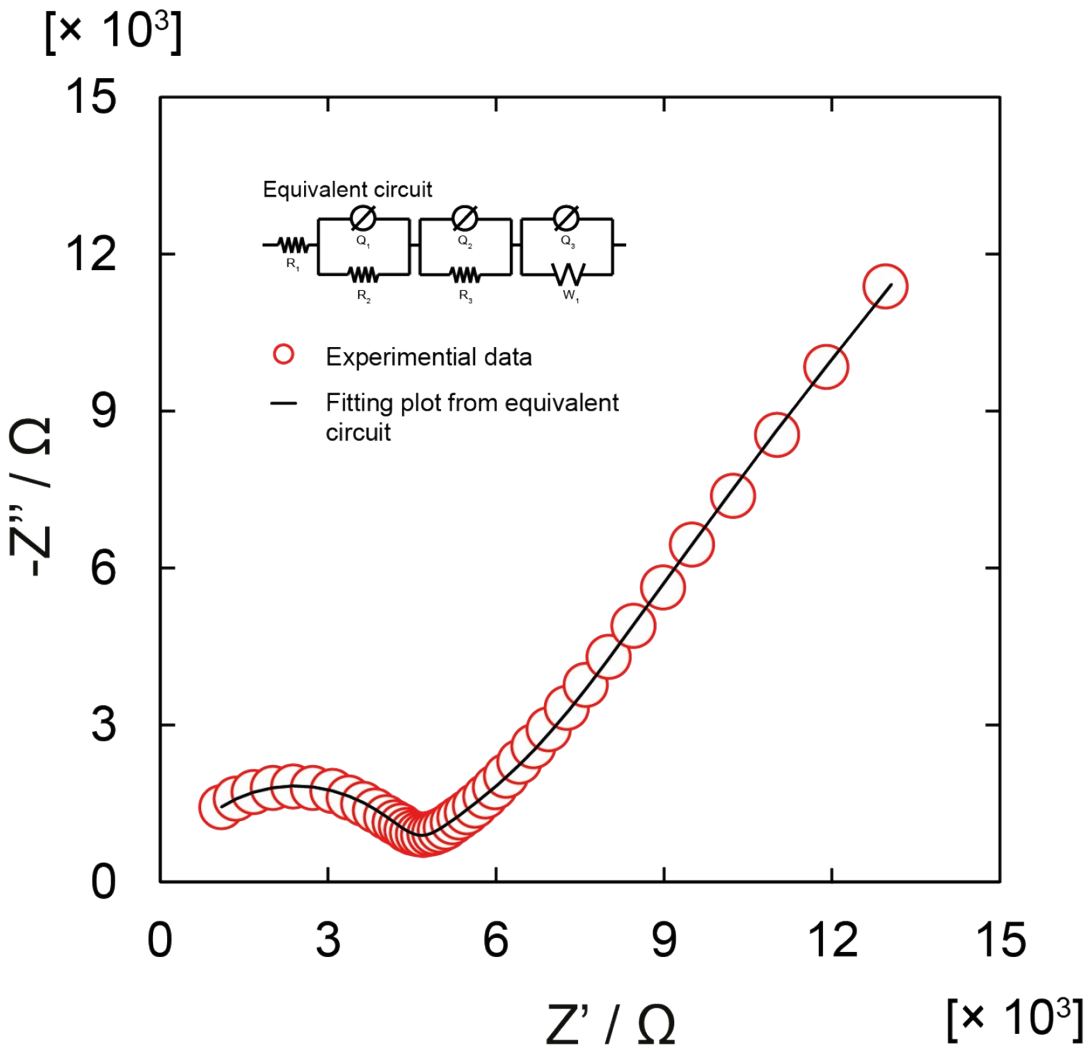

Figure S20. Nyquist plot derived from equivalent circuit (black line) and experimental Nyquist plot (red circles) of pelletized VNU-23 under 90% RH and 70 °C. Frequency ranged from 1 MHz to 10 Hz.

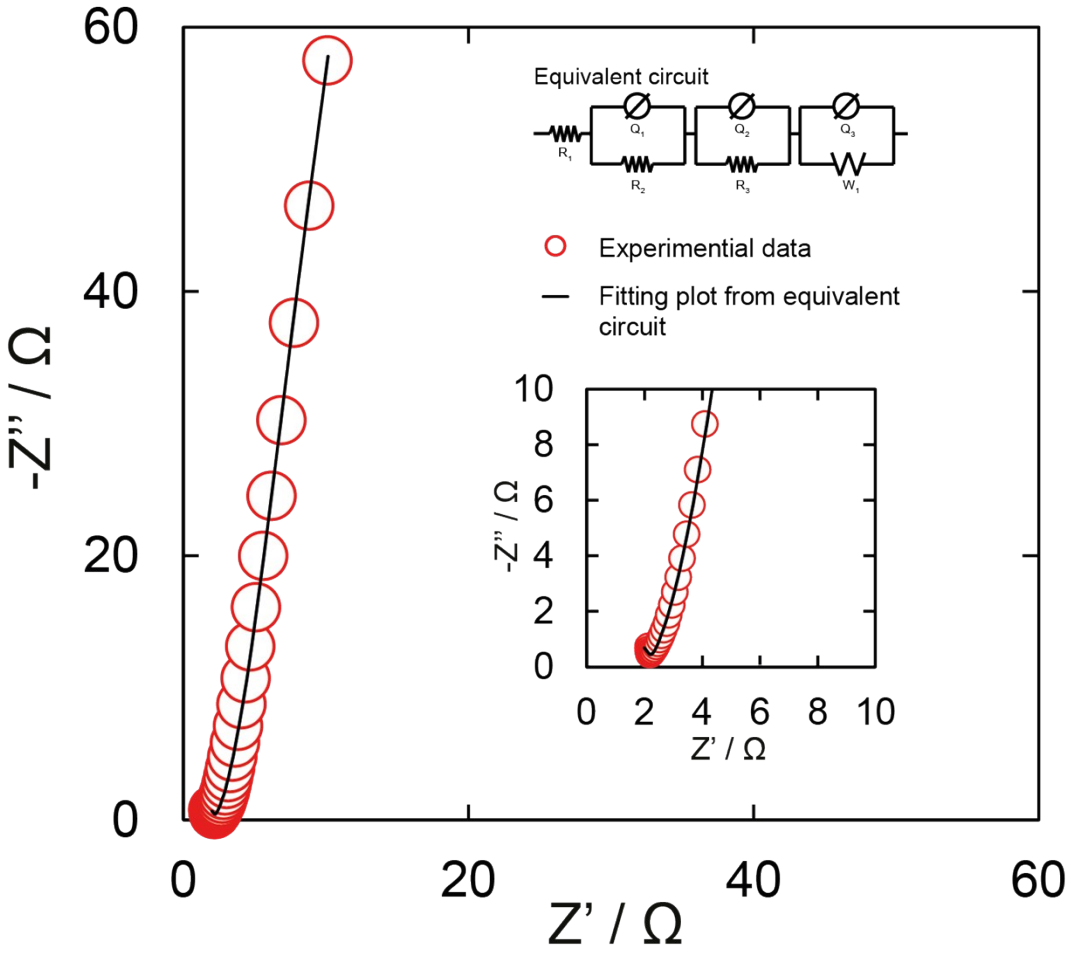

Figure S21. Nyquist plot derived from equivalent circuit (black line) and experimental Nyquist plot (red circles) of pelletized $His_{8.2}$⊂VNU-23 under 85% RH and 95 °C. Frequency ranged from 1 MHz to 10 Hz.

Table S3. Conductivity of pelletized pristine VNU-23 under 90% RH from 30 °C to 70 °C.

Temperature / °C	σ / S cm^{-1}
30	3.42×10^{-5}
40	5.45×10^{-5}
50	7.77×10^{-5}
60	1.04×10^{-4}
70	1.54×10^{-4}

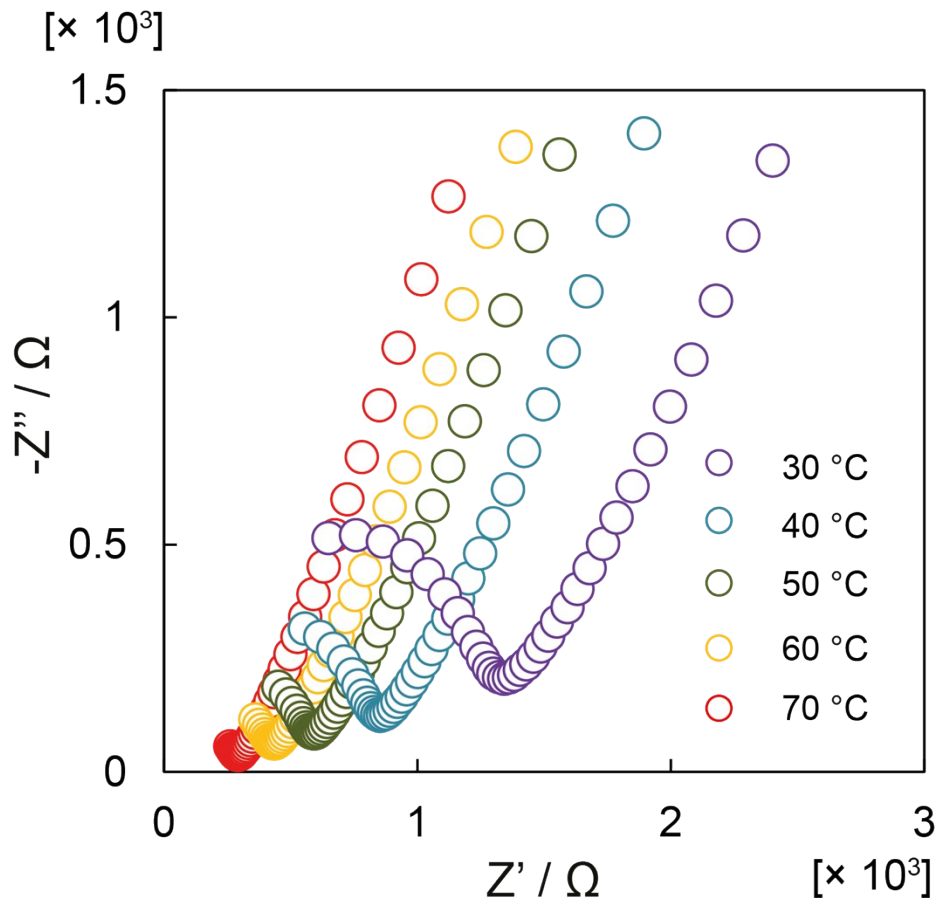

Figure S22. Nyquist plot of pelletized pristine VNU-23 under 90% RH from 30 °C to 70 °C.

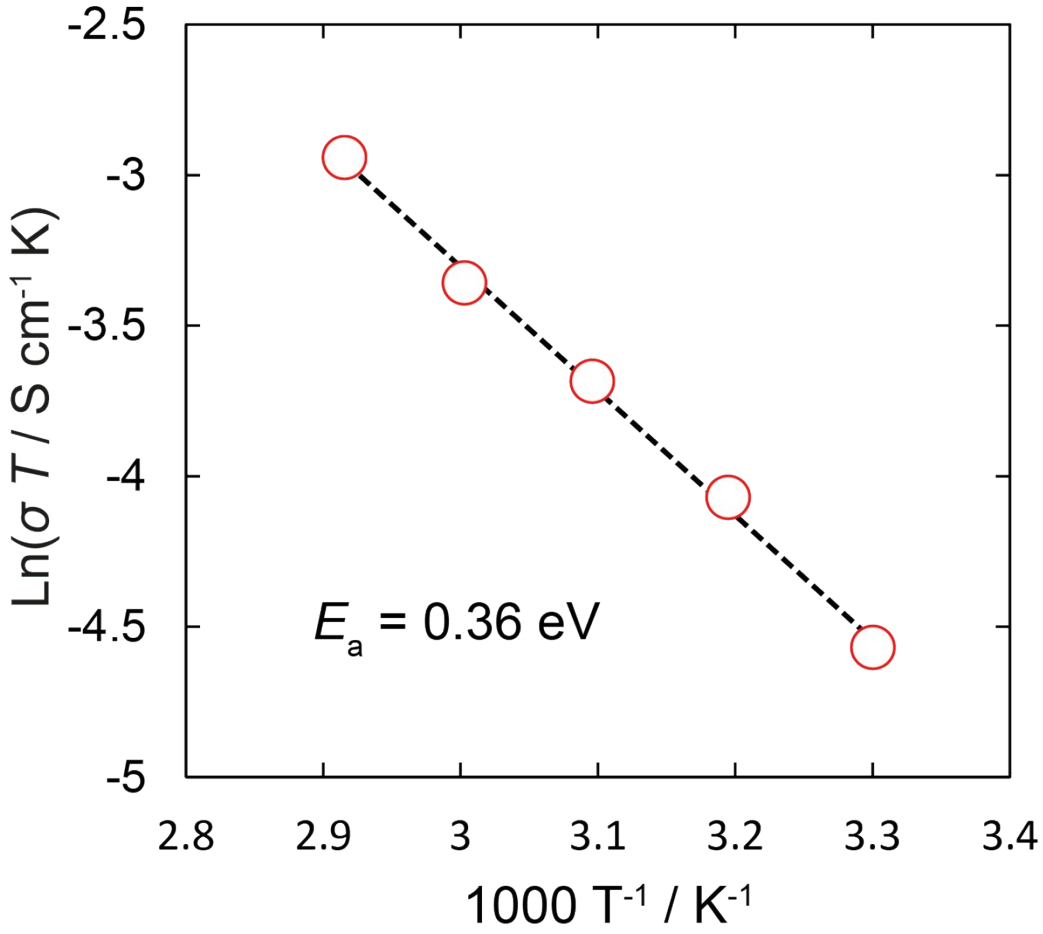

Figure S23. Arrhenius plot of pelletized pristine VNU-23 under 90% RH.

Table S4. Conductivity of pelletized VNU-23 under 90% RH from 30 °C to 70 °C.

Temperature / °C	σ / S cm^{-1}
30	1.62×10^{-6}
40	2.80×10^{-6}
50	4.43×10^{-6}
60	6.88×10^{-6}
70	1.06×10^{-5}

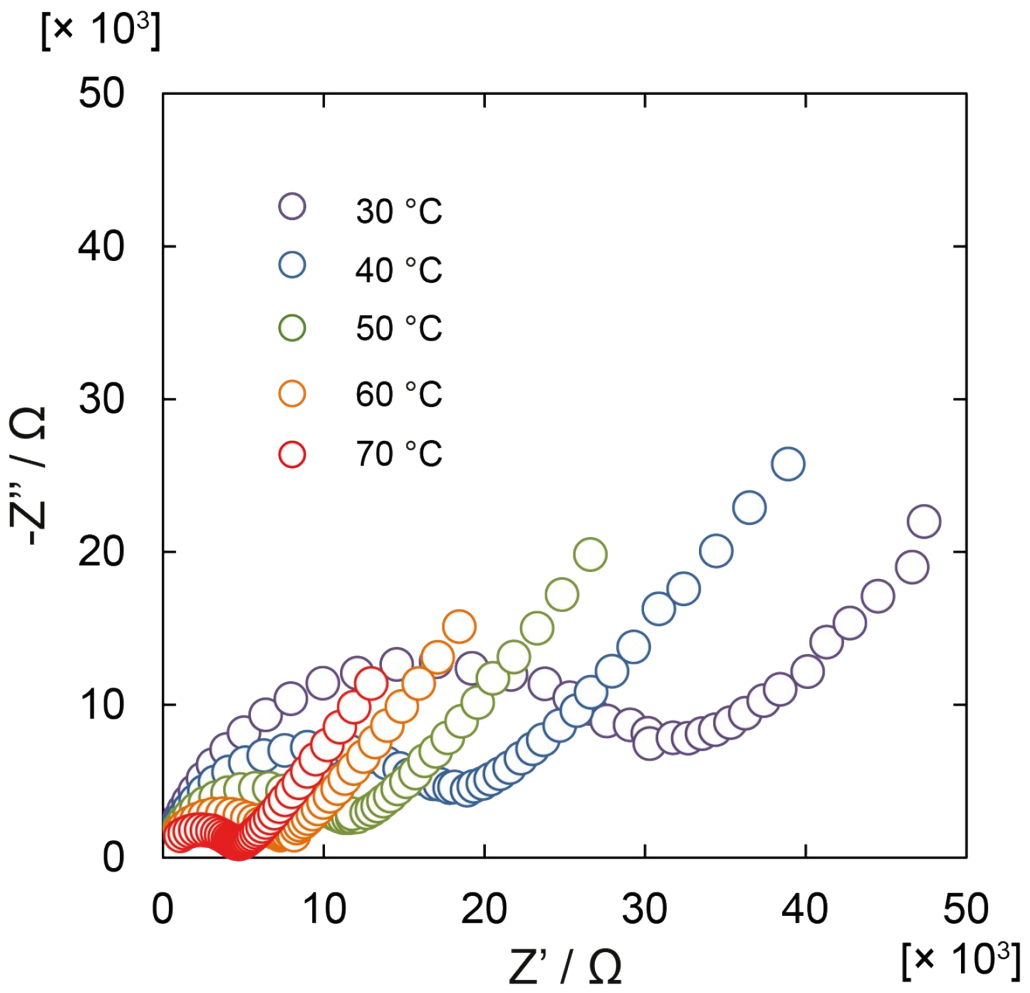

Figure S24. Nyquist plots of pelletized VNU-23 under 90% RH from 30 °C to 70 °C.

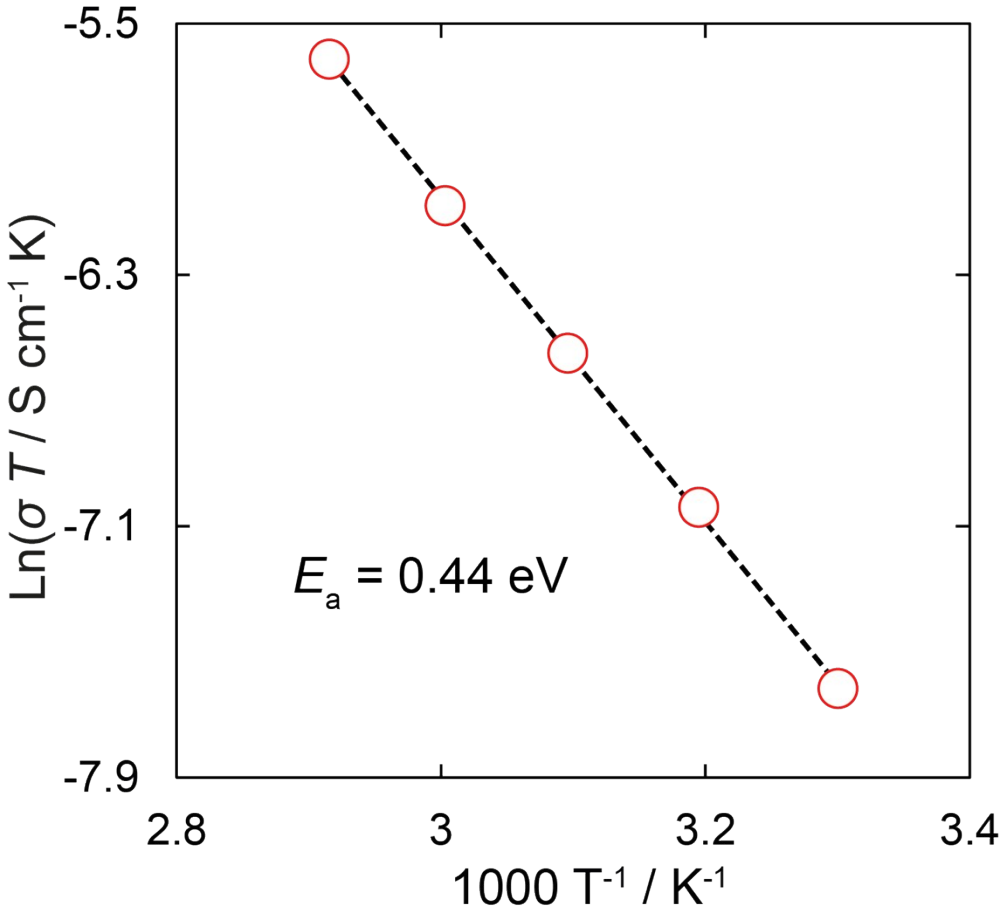

Figure S25. Arrhenius plot of pelletized VNU-23 under 90% RH.

Table S5.

Relative Humidity / %	σ / S cm^{-1}
50	1.30×10^{-6}
60	2.82×10^{-6}
70	2.27×10^{-5}
80	1.57×10^{-3}
85	1.79×10^{-2}

Conductivity of pelletized $His_{8.2}$⊂VNU-23 at 95 °C from 50% RH to 85% RH.

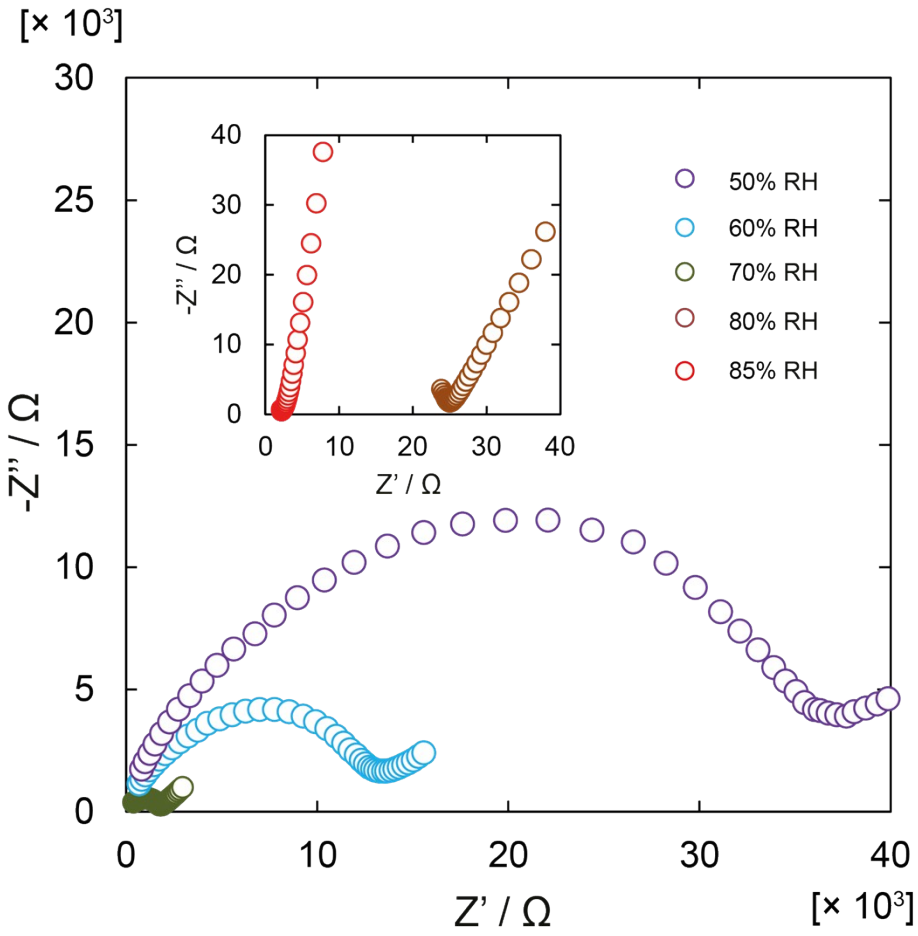

Figure S26. Nyquist plot of pelletized $His_{8.2}$⊂VNU-23 at 95 °C under relative humidity varied from 50% to 85%.

Table S6. Conductivity of pelletized $His_{8.2}$⊂VNU-23 at 85% RH with temperature from 30°C to 95 °C.

Temperature / °C	σ / S cm^{-1}
30	3.37×10^{-5}
40	8.77×10^{-5}
50	2.40×10^{-4}
60	7.99×10^{-3}
70	1.00×10^{-2}
80	1.26×10^{-2}
90	1.42×10^{-2}
95	1.65×10^{-2}

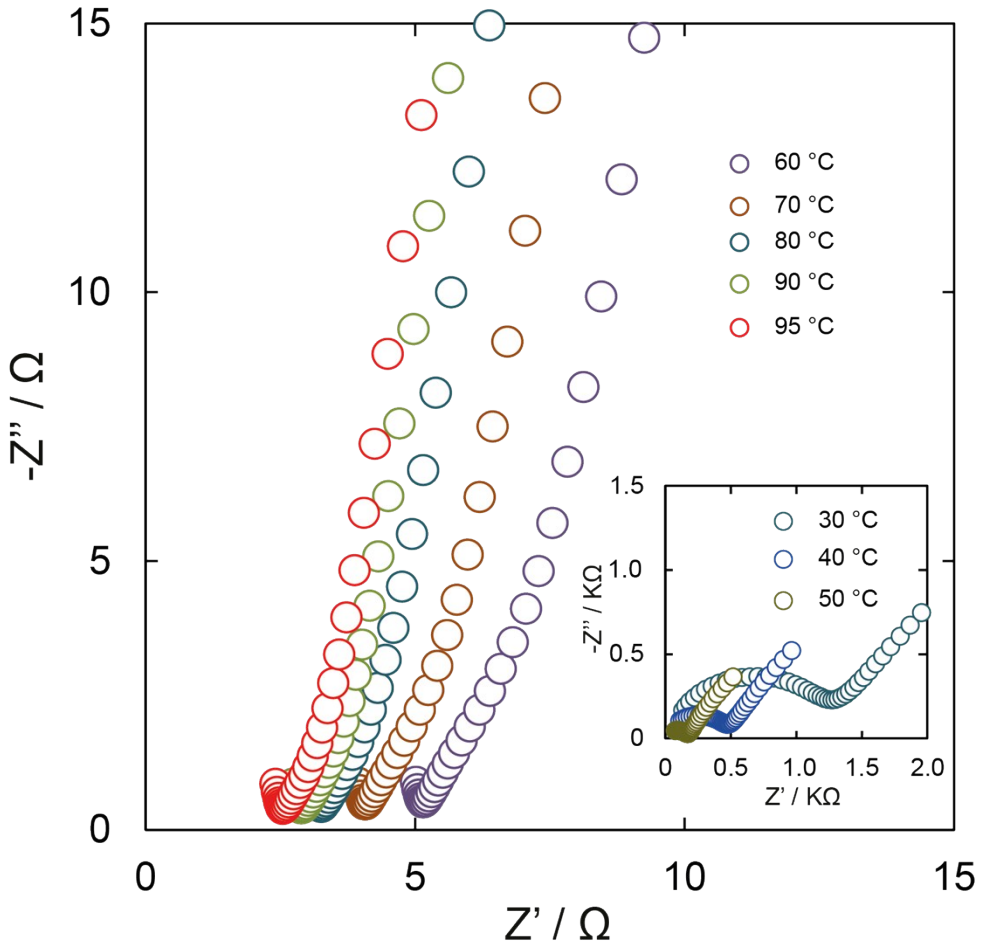

Figure S27. Nyquist plot of pelletized $His_{8.2}$⊂VNU-23 under 85% RH with temperature from 30 °C to 95 °C.

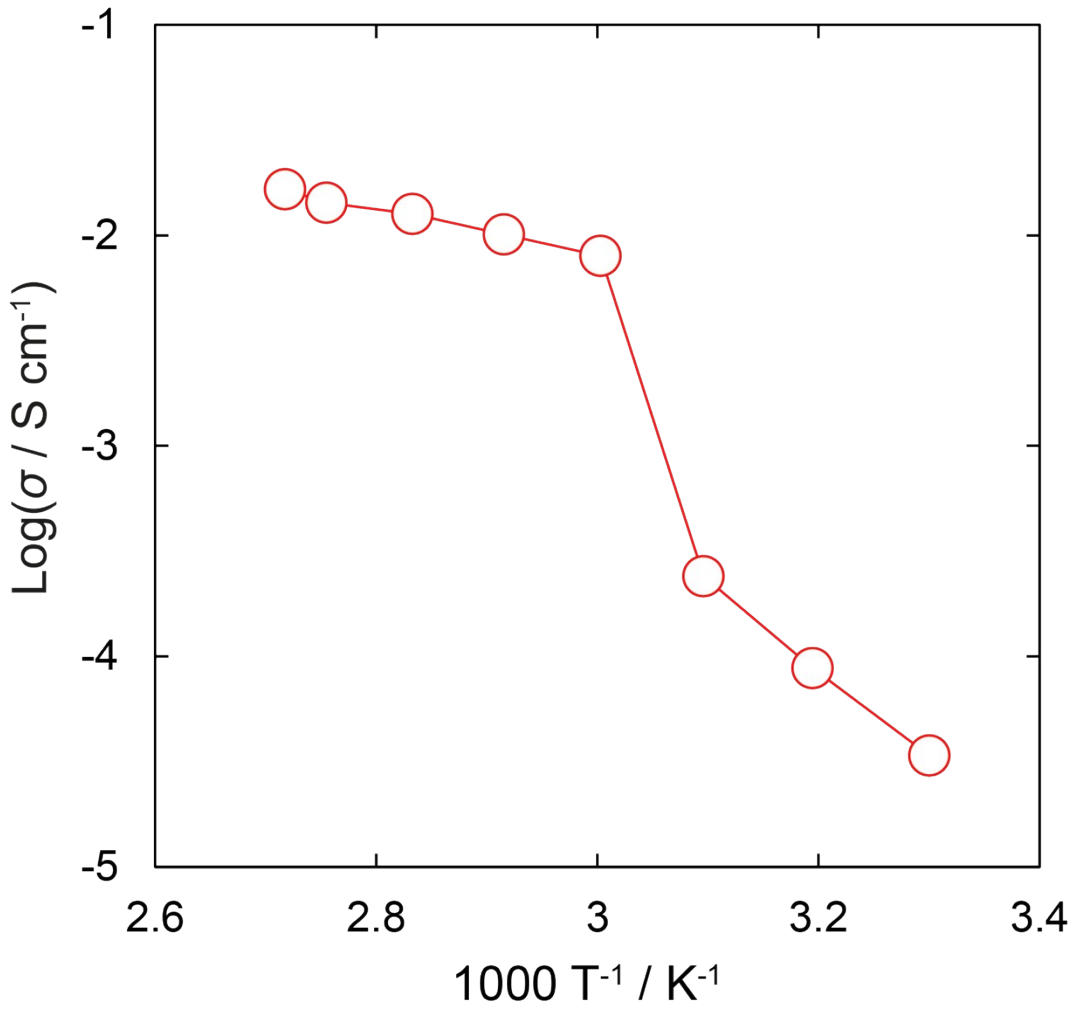

Figure S28. Temperature-dependent proton conductivity measurements (30 – 95 °C) for pelletized $His_{8.2}$⊂VNU-23 under 85% RH.

Table S7. Cycling measurements for proton conductivity of pelletized $His_{8.2}$⊂VNU-23 at 85% RH with

Temperature / °C	σ / S cm^{-1}	
	Heating	Cooling
60	8.74×10^{-3}	
70	1.17×10^{-2}	1.15×10^{-2}
80	1.50×10^{-2}	1.46×10^{-2}
90	1.79×10^{-2}	1.77×10^{-2}
95	1.97×10^{-2}	1.96×10^{-2}

temperature from 60 °C to 95 °C.

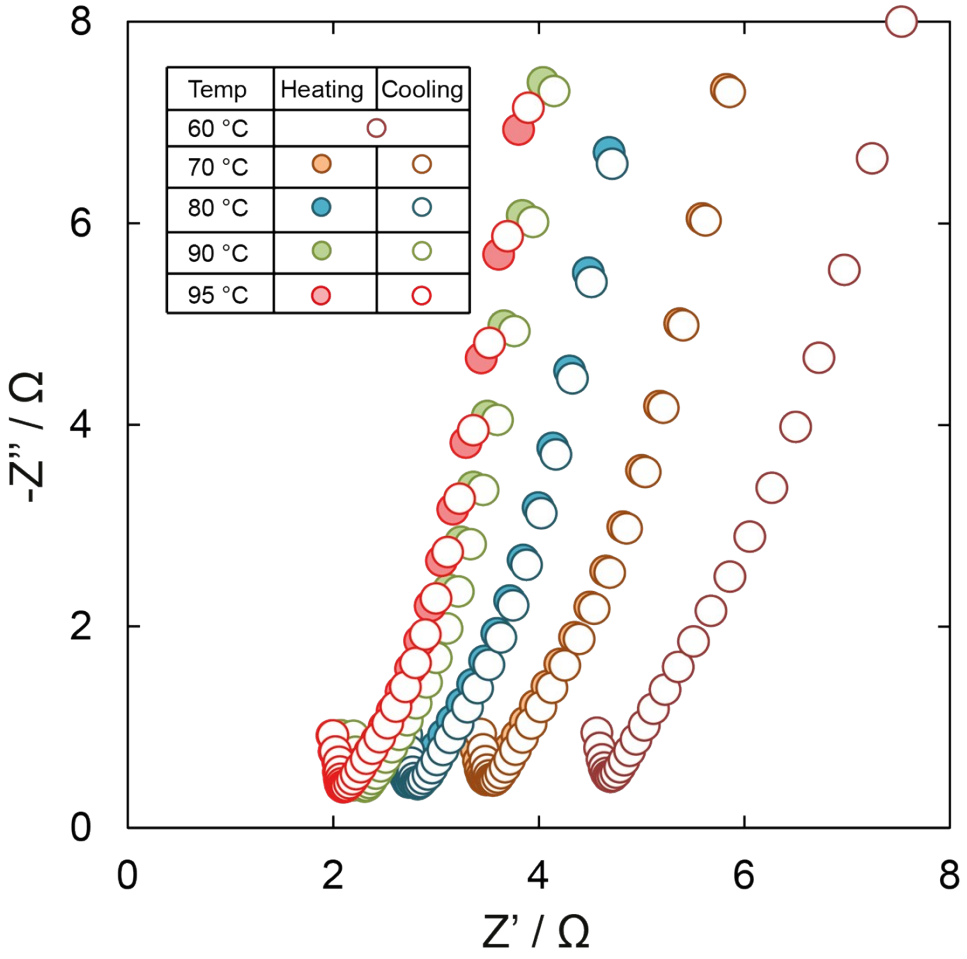

Figure S29. Nyquist plot for cycling measurements of pelletized $His_{8.2}$⊂VNU-23 at 85% RH with temperature ranged from 60-95 °C.

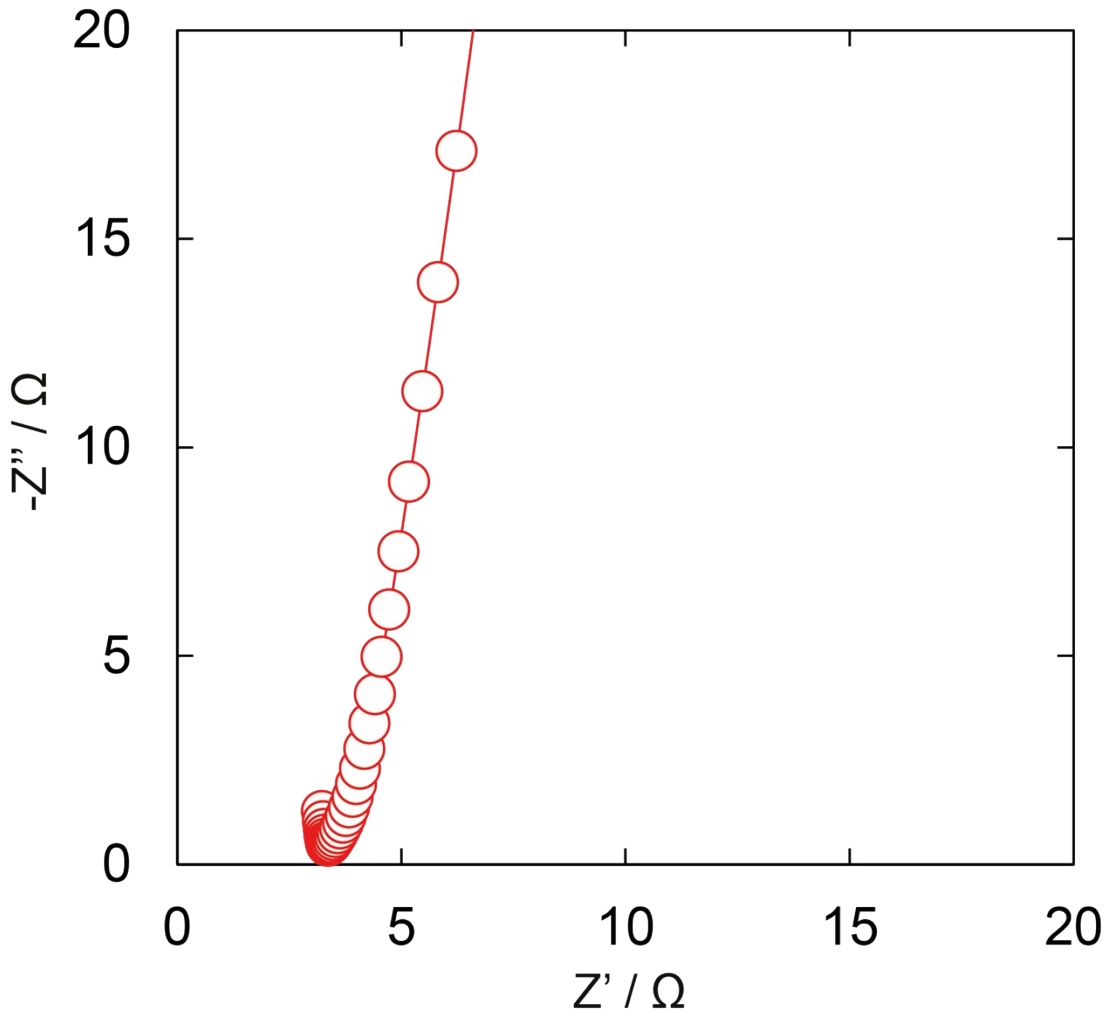

Figure S30. Nyquist plot of pelletized $His_{8.2}$⊂VNU-23 under 85% RH and 95 °C after 120 hours of consecutive ac impedance measurements.

Section S15. Stability of $His_{8.2}$⊂VNU-23 during Proton Conductivity Studies

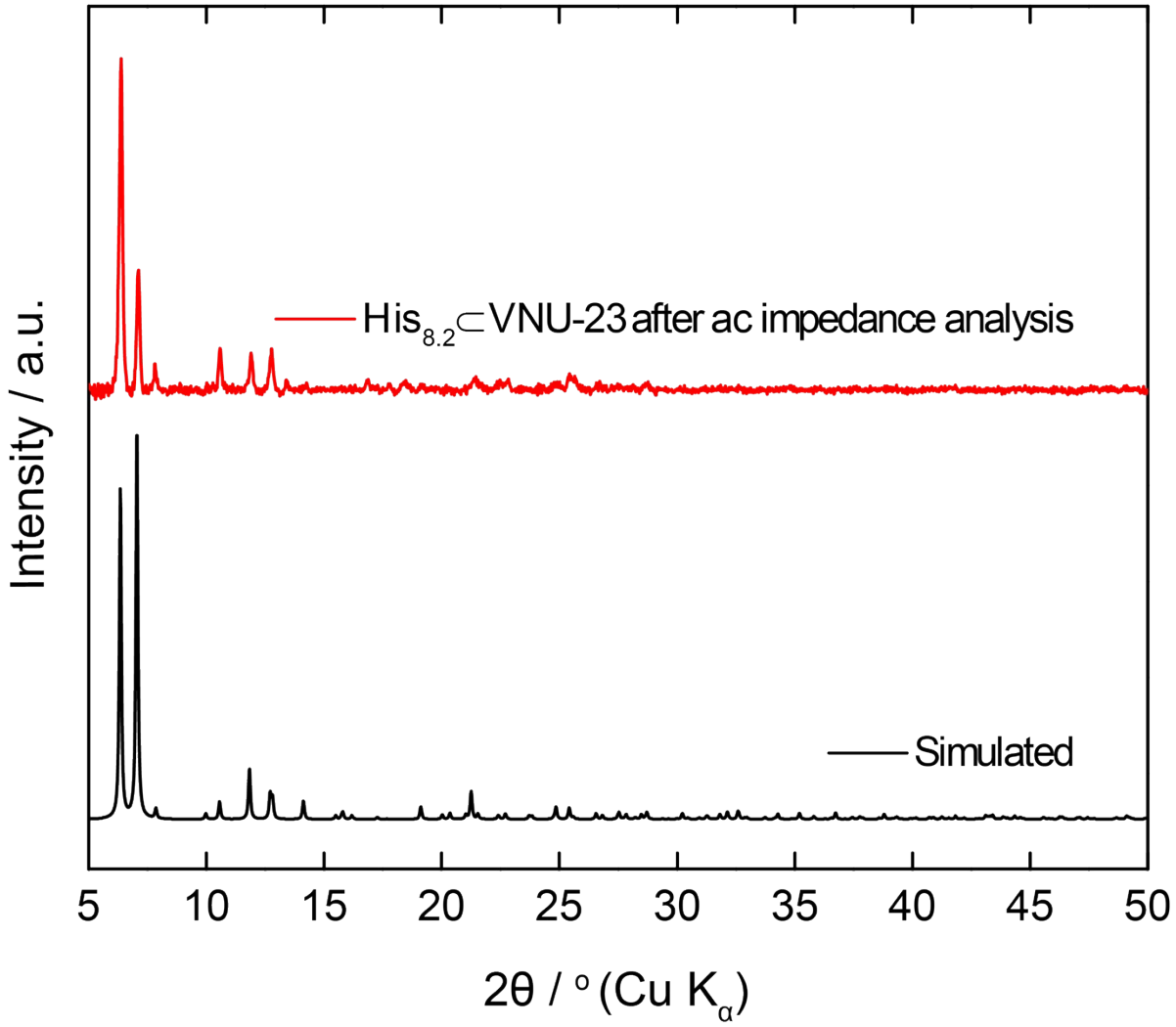

Figure S31. Simulated PXRD pattern of VNU-23 (black) as compared to the experimental pattern from the subjecting pelletized $His_{8.2}$⊂VNU-23 to time-dependent ac impedance measurements at 85% RH and 95 °C for 120 hours (red).

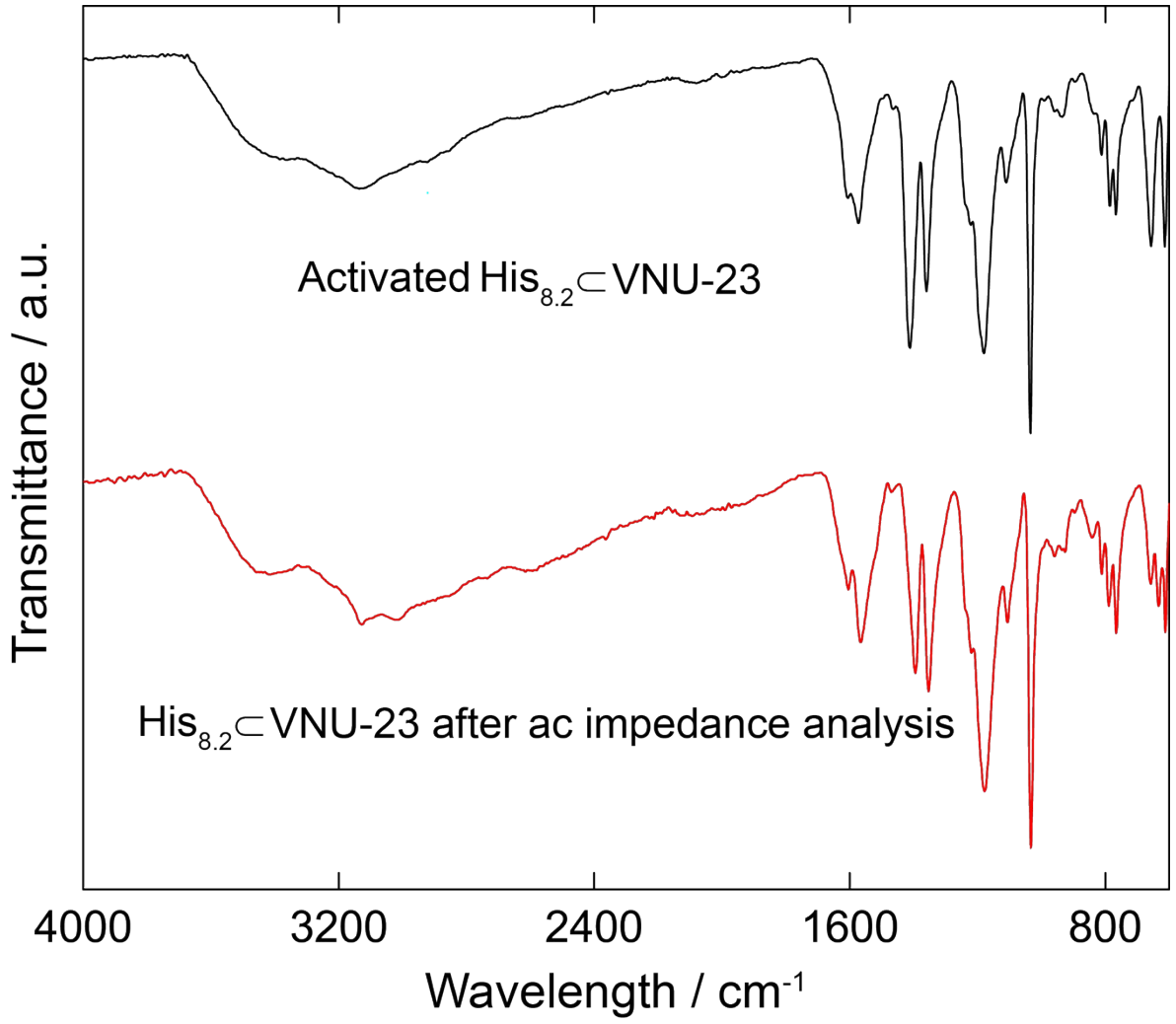

Figure S32. FT-IR of activated $His_{8.2}$⊂VNU-23 (black) in comparison with $His_{8.2}$⊂VNU-23 after ac impedance analysis (red).